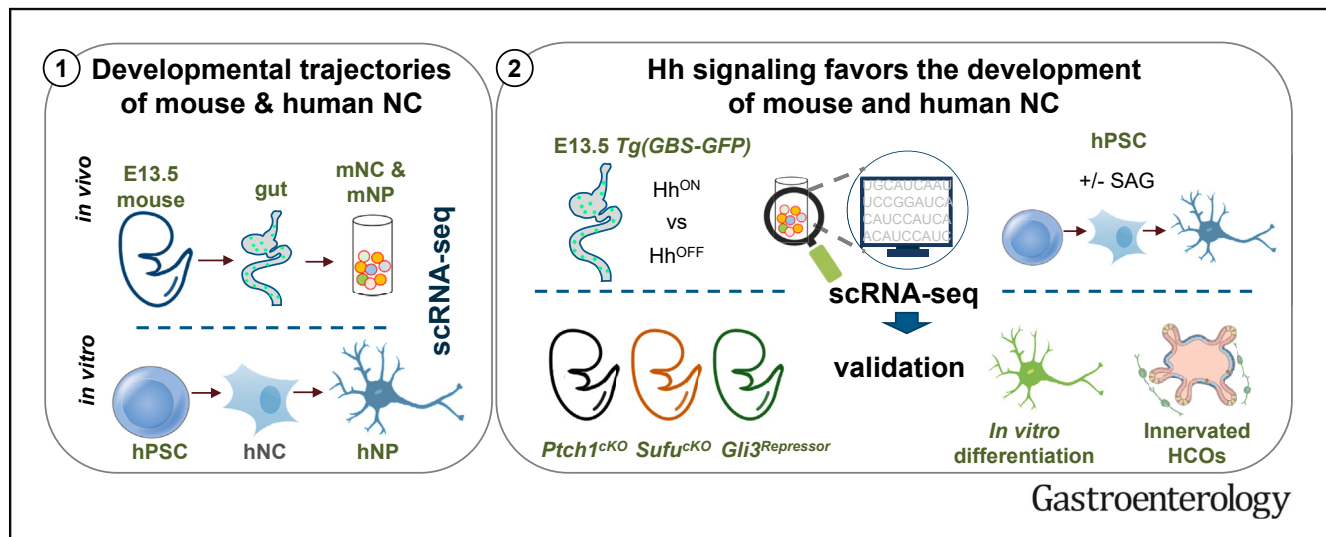




Activation of Hedgehog Signaling Promotes Development of Mouse and Human Enteric Neural Crest Cells, Based on Single-Cell Transcriptome Analyses

Sin-Ting Lau,^{1,2} Zhixin Li,^{1,2} Frank Pui-Ling Lai,^{1,2} Kathy Nga-Chu Lui,¹ Peng Li,¹ Jorge O. Munera,³ Guangjin Pan,⁴ Maxime M. Mahe,^{5,6} Chi-Chung Hui,^{7,8} James M. Wells,³ and Elly Sau-Wai Ngan¹

¹Department of Surgery, Li Ka Shing Faculty of Medicine, Pokfulam, Hong Kong; ²Dr Li Dak Sum Research Centre, University of Hong Kong, Pokfulam, Hong Kong; ³Division of Developmental Biology, Cincinnati Children's Hospital Research Foundation, Cincinnati, Ohio; ⁴CAS Key Laboratory of Regenerative Biology, Guangzhou Institutes of Biomedicine and Health, China; ⁵Division of Pediatric General and Thoracic Surgery, Cincinnati Children's Hospital Research Foundation, Cincinnati, Ohio; ⁶INSERM UMR 1235-TENS, INSERM, University of Nantes, Nantes, France; and ⁷Program in Developmental and Stem Cell Biology, Toronto, Ontario, Canada; and ⁸The Hospital for Sick Children, and Department of Molecular Genetics, University of Toronto, Toronto, ON, Canada



BACKGROUND & AIMS: It has been a challenge to develop fully functioning cells from human pluripotent stem cells (hPSCs). We investigated how activation of hedgehog signaling regulates derivation of enteric neural crest (NC) cells from hPSCs.

METHODS: We analyzed transcriptomes of mouse and hPSC-derived enteric NCs using single-cell RNA sequencing (scRNA-seq) to identify the changes in expression associated with lineage differentiation. Intestine tissues were collected from *Tg(GBS-GFP)*, *Sufu*^{f/f}; *Wnt1-cre*, *Ptch1*^{+/−}, and *Gli3*^{Δ699/Δ699} mice and analyzed by flow cytometry and immunofluorescence for levels of messenger RNAs encoding factors in the hedgehog signaling pathway during differentiation of enteric NCs. Human NC cells (*HNK-1*⁺*p75^{NTR}*⁺) were derived from IMR90 and UE02302 hPSC lines. hPSCs were incubated with a hedgehog agonist (smoothed agonist [SAG]) and antagonists (cyclopamine) and analyzed for differentiation. hPSC-based innervated colonic organoids were derived from these hPSC lines and analyzed by immunofluorescence and neuromuscular coupling assay for expression of neuronal subtype markers and

assessment of the functional maturity of the hPSC-derived neurons, respectively. **RESULTS:** Single-cell RNA sequencing analysis showed that neural fate acquisition by human and mouse enteric NC cells requires reduced expression of NC- and cell cycle-specific genes and up-regulation of neuronal or glial lineage-specific genes. Activation of the hedgehog pathway was associated with progression of mouse enteric NCs to the more mature state along the neuronal and glial lineage differentiation trajectories. Activation of the hedgehog pathway promoted development of cultured hPSCs into NCs of greater neurogenic potential by activating expression of genes in the neurogenic lineage. The hedgehog agonist increased differentiation of hPSCs into cells of the neuronal lineage by up-regulating expression of GLI2 target genes, including *INSM1*, *NHLH1*, and various bHLH family members. The hedgehog agonist increased expression of late neuronal markers and neuronal activities in hPSC-derived neurons. **CONCLUSIONS:** In enteric NCs from humans and mice, activation of hedgehog signaling promotes differentiation into neurons by promoting cell-state transition,

expression of genes in the neurogenic lineage, and functional maturity of enteric neurons.

Keywords: Enteric Nervous System; Regenerative Medicine; Hirschsprung Disease; Disease Model.

Aberrant neural crest (NC) development results in a myriad of birth defects and diseases, such as Hirschsprung disease attributed to the developmental defects of enteric NC. Directed differentiation protocols for derivation of NC from human pluripotent stem cells (hPSCs) have been established by various research groups and used for disease modeling and regenerative medicine studies.^{1–4} The existing protocols to differentiate hPSCs into NC are mainly based on the modulation of known inductive signals implicated in early NC development.^{4–6} Overall, this approach can generate NC cells with distinct fate potentials along various axial levels. However, NC cells obtained through this approach are usually heterogeneous, and their neurogenic potential varies across different hPSC lines, a problem that may necessitate the addition of other factors to further boost the neurogenic fate potential of these cells. Currently, there is limited understanding of the molecular events underlying the hPSC-to-NC transition and their subsequent neuronal lineage differentiation. It is also unclear whether manipulation of other developmental pathways known to act during the later stage of NC development will improve the speed and efficiency of neural fate acquisition.

Hedgehog acts as a morphogen to specify progenitor cell identity and neuronal fate in the ventral neural tube, and hedgehog pathway agonists (such as smoothened agonist [SAG]) have been widely used to improve the derivation of midbrain and hindbrain motoneurons from hPSCs through improving the survival and neural fate acquisition of the progenitors.⁷ Mutant studies in mice suggest that hedgehog signaling regulates the differentiation of enteric NC during the development of enteric nervous system (ENS), and aberrant hedgehog pathway activation induces premature differentiation of enteric NC, leading to an abnormal neuron-to-glia ratio.^{5,8} Nevertheless, how the dynamic hedgehog signal directs the differentiation of the enteric NC remains elusive.

The latest high-resolution RNA sequencing (RNA-seq) technology allows a comprehensive analysis of the lineage commitment process after the embryonic stem cells exit their pluripotent state and of the timing of various differentiation cues underlying the generation of cell-type diversity⁹ and the *in vivo* differentiation trajectories of progenitors during mouse embryogenesis.^{10–12} NC derivation from hPSCs and their subsequent differentiation toward neuronal lineage involve multiple steps, and the resulting NC cells and their neuronal derivatives are likely heterogeneous, such that cells at intermediate differentiation states may resemble NC cells at distinct developmental stages *in vivo*.¹³ Therefore, we anticipate that analyzing the transcriptomes of mouse- and hPSC-derived NC cells and their neuronal derivatives at the single-cell level may reveal

WHAT YOU NEED TO KNOW

BACKGROUND AND CONTEXT

It has been a challenge to develop fully functioning cells from human pluripotent stem cells (hPSCs).

NEW FINDINGS

The authors identified the developmental trajectories of human and mouse enteric NCs using single-cell transcriptomic analyses. Hedgehog stimulation promotes the cell state progression of human and mouse enteric NCs.

LIMITATIONS

The authors tested the effects of hedgehog stimulation on the development of enteric NCs using only mouse and human NCs and colonic organoids derived from 2 independent hPSC lines.

IMPACT

Improving the neural fate differentiation efficiency of hPSC-derived NC cells will expedite the application of these cells in regenerative medicine.

the lineage-specifying signals underlying these developmental events; we hope that information will guide optimization of the differentiation protocol for the generation of fully functioning NC in a systematic way.

Improving the neural fate differentiation efficiency of hPSC-derived NC cells will expedite the application of these cells in regenerative medicine, such as replenishing the missing neurons in the colon of patients with Hirschsprung disease. hPSC-derived organoids represent near-physiologic models, bridging *in vitro* research and clinical medicine. A protocol for the differentiation of human intestinal organoids from hPSCs was established recently.¹⁴ hPSC-derived human intestinal organoids contained all functional tissue units, including a functional ENS, and resembled the native tissue architecture of the small intestine. In addition, human colonic organoids (HCOs) resembling the posterior bowel could be generated by using a similar approach with a brief activation of the bone morphogenetic protein (BMP) pathway. Even though the reported HCOs did not contain ENS, they exhibited molecular, cellular, and morphologic properties of the human colon.⁶ Taken together, the latest advances in organoid-based technologies raise the

Abbreviations used in this paper: BP, bipotent progenitor; D20, day 20; D40, day 40; DEG, differentially expressed gene; E, embryonic day; ENCC, enteric neural crest-derived cell; ENS, enteric nervous system; FACS, fluorescence-activated cell sorting; GBS, GLI-binding sequence; GFP, green fluorescent protein; GP, glial progenitor; HCO, human colonic organoid; hPSC, human induced pluripotent cell; hNC, human neural crest; hNP, human neuronal progenitors; hPSC, human pluripotent stem cell; NC, neural crest; NF, neurofilament; PCA, principal component analysis; PGP, protein gene product; RNA-seq, RNA sequencing; SAG, smoothened agonist; scRNA-seq, single-cell RNA sequencing; TF, transcription factor; TH, tyrosine hydroxylase; VIP, vasoactive intestinal polypeptide.

 Most current article

© 2019 by the AGA Institute
0016-5085/\$36.00

<https://doi.org/10.1053/j.gastro.2019.08.019>

important possibility of using an innervated HCO model to appraise the therapeutic value of hPSC-derived NC cells.

In this study, we applied single-cell RNA-seq (scRNA-seq) to establish the differentiation trajectories of mouse and human enteric NC. Our analysis showed that hPSC-derived NC cells give rise to neuronal progenitors resembling the developing ENS in embryonic day (E)-13.5 mouse guts, where numerous neuronal intermediates are emerging, representing the key developmental window for the early-born enteric neurons. Dynamic hedgehog signaling directs the progression of mouse enteric NC along the differentiation path *in vivo*. Concordantly, activation of the hedgehog pathway alters the topology of the neuronal differentiation path of human enteric NC and primes NC toward the neurogenic lineage. The involvement of hedgehog signaling in the transition from hPSCs to the NC lineage and the subsequent neuronal lineage differentiation were also directly illustrated using chemical modulation of hedgehog signaling and *in vitro* models based on cells and on our newly established innervated HCOs.

Methods

Mice

Tg(GBS-GFP), *Sufu^{ff}*, *Gli3^{A699}*, *Ptch1^{ff}*, *b3-IIla-Cre*, and *Wnt1-Cre* mice were previously generated.^{8,15–18} NOD/SCID mice were purchased from our animal unit. Genotyping was performed with the primers listed in *Supplementary Table 1*. All experiments were performed in accordance with procedures approved by the Committee on the Use of Live Animals, University of Hong Kong (CULTRA 2827-15, 3837-15, and 4181-16).

Human Induced Pluripotent Stem Cells, Human Neural Crest, and Human Neuronal Progenitors

A control human induced pluripotent stem cell (hiPSC) line (IMR90-iPSC) was obtained from WiCell Research Resources (Madison, WI). Another control hiPSC cell line (UE02302) was generated from urine-derived cells of a male individual by episomal reprogramming vectors carrying the 4 reprogramming factors.¹⁹ All hiPSCs used in this study were maintained on a Matrigel-coated (BD Biosciences, Franklin Lakes, NJ) plate with mTeSR1 medium (StemCell Technologies, Vancouver, British Columbia, Canada). Human NC (hNC) cells were derived from hiPSCs and enriched by fluorescence-activated cell sorting (FACS) as described previously.^{1,20} The neuronal differentiation started with culturing the FACS-sorted hNC cells in N2 medium containing brain-derived neurotrophic factor (BDNF), glial cell linederived neurotrophic factor (GDNF), neurotrophin-3 (NT-3), nerve growth factor (NGF) and cyclic adenosine monophosphate (cAMP). NC-derived neurons at differentiation day 9 were fixed for immunocytochemistry analysis, and neurons at days 20 (NP-D20) and 40 (NP-D40) were harvested by using Accutase (Millipore, Billerica, MA) for scRNA-seq.

Derivation of Human Colonic Organoids From Human Induced Pluripotent Cell Line

hNCs (enteric neural crest-derived cells [ENCCs]) were generated as described, and HCOs were generated according

to the published protocol.⁶ ENCCs and HCOs were combined at an early stage of colon differentiation. HCOs plus ENCCs were ectopically transplanted into the kidney capsule of NOD/SCID mice to obtain mature HCO explants, as previously described.¹⁴ Engrafted HCOs were harvested 8–10 weeks after transplantation and subjected to immunohistochemistry for the detection of neural, glial, and colon cells or used for *ex vivo* neuromuscular coupling tests.

Fluorescence-activated cell sorting and flow cytometric analysis

For mouse enteric NC, guts were isolated from E13.5 *Wnt1-Cre; YFP* and *Tg(GBS-GFP)* embryos and digested with dispase/collagenase. Mouse enteric NCs were detected with p75^{NTR} antibody and green fluorescent protein (GFP). For hNCs, the 10-day-differentiated cells were dissociated with Accutase and then incubated with APC-HNK-1 and FITC-p75^{NTR} antibodies (*Supplementary Table 2*). Labeled NCs were analyzed or isolated with BD FACSAria III Cell Sorter (BD Biosciences).

Immunofluorescence analysis

Cells, mouse embryos, HCOs, and HCO explants were fixed in 4% paraformaldehyde in phosphate-buffered saline. Embryos and HCO explants embedded in optimum cutting temperature compound (Tissue-Tek; Sakura/Tissue-Tek Company, Torrance, CA) or paraffin and sectioned. The fixed cells and sections were rehydrated, stained with the antibodies against various colon or neuronal markers (*Supplementary Table 2*) and photographed with a Carl Zeiss (Oberkochen, Germany) LSM780 or LSM810 confocal microscope. Quantitative image analysis of differentiated neuronal cultures was performed with ImageJ software (National Institutes of Health, Bethesda, MD). A minimum of 4,000 cells were analyzed per sample.

Single-cell RNA sequencing

Single-cell transcriptomes of human and mouse cells were obtained by using the plate- and droplet-based scRNA-seq platforms with the Smart-seq v4 (Clontech, Mountain View, CA) and 10 \times Genomics (Pleasanton, CA) kits, respectively. The library construction and sequencing were performed at the Centre of Genomic Science, University of Hong Kong. Human and mouse cells were visualized by principal component analysis (PCA) and t-distributed stochastic neighbor embedding by using the prcomp and Rtsne R package, version 3.5.0. Single-cell pseudotime analyses were performed with the SPRING²¹ algorithm and by principal.curve (R package). Spearman correlation was calculated between human clusters and mouse clusters based on the homologous genes along the pseudotime. Differentially expressed genes (DEGs) were identified by SCDE.²² Overrepresentation analysis of the DEGs was based on the Gene Ontology and Kyoto Encyclopedia of Genes and Genomes database using the clusterProfiler R package.²³ All annotated code showing key steps of the analysis are available on GitHub at <https://github.com/ellylab/HCO-paper>.

Experimental details are available in the *Supplementary Methods*.

Results

Human Pluripotent Stem Cell-Derived Neural Crest Cells Resembles the Mouse Developing Enteric Nervous System

To define the cell types of the hPSC-derived NC derivatives and their developmental stages relative to the mouse model, we performed scRNA-seq to examine the gene expression dynamics along human and mouse enteric NC development. In brief, human NC cells were derived from 2 control hPSC lines (IMR90 and UE02302) by using the stepwise differentiation protocol with dual-SMAD inhibitors, followed by caudalization with retinoic acid to obtain posterior NC cells (hNC), as detailed in our previous study.¹ NC cells were then enriched FACS with HNK-1 and p75^{NTR} antibodies and cultured in the neuronal differentiation medium for 20 and 40 days, respectively, to obtain the early (human neuronal progenitor [hNP]-D20) and late (hNP-D40) neuronal progenitors (Figure 1A). In total, we quantified the transcriptional profiles of 384 hPSCs (IMR90 and UE02302), 782 control hNC cells, and 792 hNP-D20 and 768 hNP-D40 progenitors (Supplementary Figure 1). In mice, E13.5 represents a key window for early ENS, and profiling of 120 single-cell enteric NC transcriptomes at this stage showed 2 distinct differentiation paths of enteric NC for the neuronal and glial lineages.²⁴ To better define various neuronal intermediates that emerged along the neuronal differentiation trajectory, we further sequenced the transcriptomes of 7671 mouse enteric NC cells and their derivatives isolated from E13.5 (*Wnt1-cre;YPF*) embryonic guts and used them for the subsequent comparisons (Supplementary Figure 1).

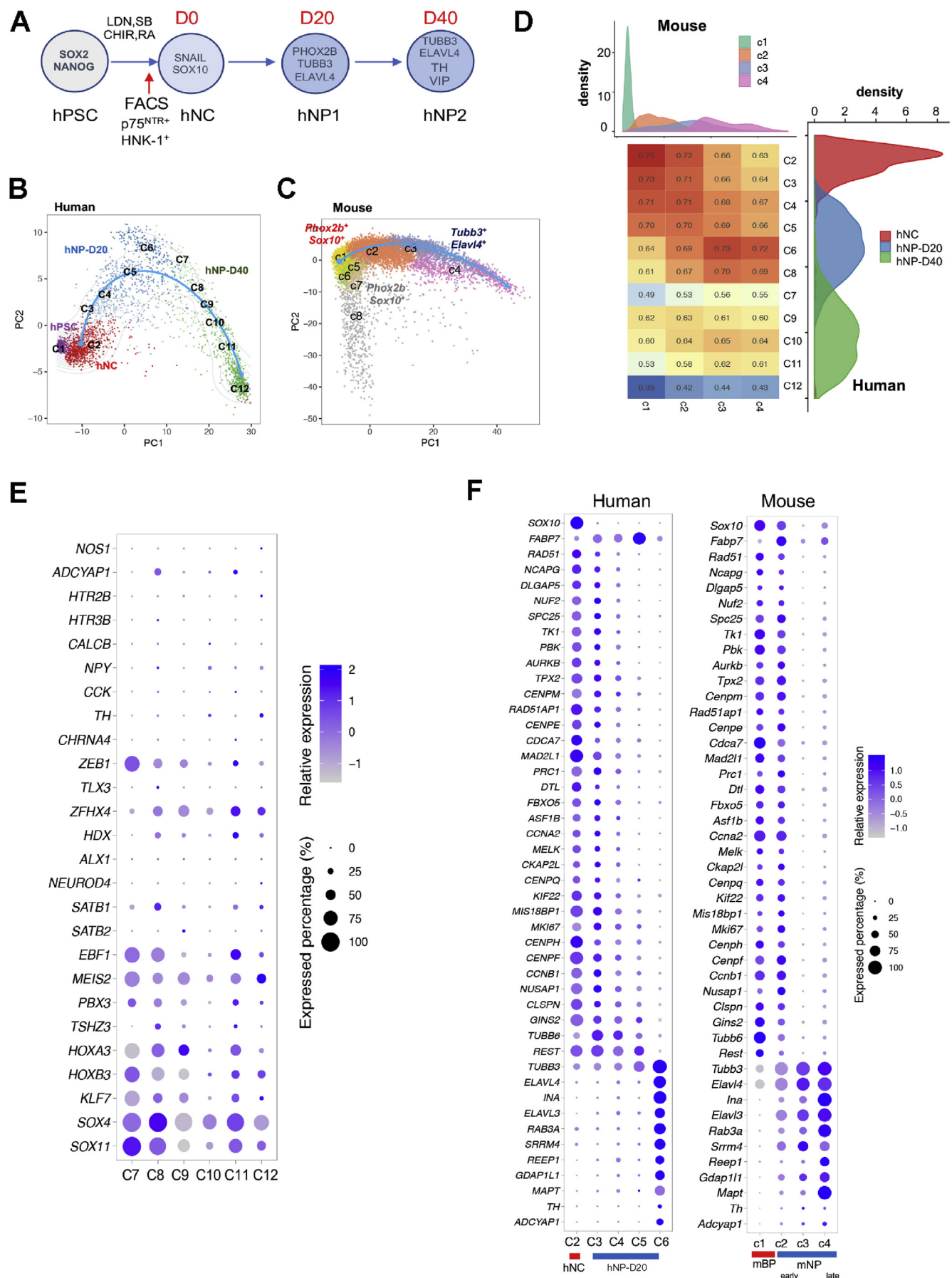
We first used PCA to visualize gene expression dynamics during the hPSC-to-NC-to-neuron transition and in a snapshot of early mouse ENS development at the single-cell level. PCA mapped the expression profiles of individual cells within the cell pool on a 2-dimensional space and placed cells with similar expression profiles in proximity to each other. Twelve (C1–12) and 8 (c1–8) distinct clusters were identified from human and mouse cell pools, respectively (Figure 1B and C). Clusters 2–12 represented the neuronal lineage differentiation trajectory of hNC (Figure 1B). Consistent with the previous finding,²⁴ the mouse cell pool contained cells at varying points along the developmental progression, such that PCA showed 2 distinct NC differentiation trajectories for neuronal and glial lineages. Eight distinct clusters were identified, representing the main neuronal and glial populations in E13.5 embryonic guts. As illustrated in Figure 1C and Supplementary Figure 2, the differentiation trajectory of mouse enteric NC for the neuronal lineage began with the mouse bipotent progenitors (BPs) (mBP; c1), passed through 2 intermediates inferred using PCA (mNP_{early}; c2 and c3), and terminated at a more mature neuron state (mNP_{late}; c4; *Tubb3*^{high}, *Elavl4*^{high}). Another distinct population of progenitors (c8) was found, and these cells coexpressed a unique NC invasion signature (*Acta2*^{high}, *Actg2*^{high}, *Tagn*^{high}, *Hand1*^{high}, *Snail2*^{high}, *Sox10*^{low}) that were previously identified from the migratory font of NC stream in an avian model,²⁵ resembling the highly migratory

population of NC cells (Supplementary Figure 2). Three populations of glial progenitors (GPs) (mGP; c5, c6, and c7) expressing the early glial markers (*Fabp7*, *Plp1*, and *Sox10*) were also identified.

We arranged the clusters belonging to the neuronal lineage (human C2–C12 and mouse c1–c4) in pseudotime manner and then compared the developmental trajectories of human and mouse NC by performing a Spearman correlation analysis to estimate the similarity of the overall gene expression profiles in these clusters. As shown in Figure 1D, strong similarities were observed between mouse c1–c2 and human C2–C5, corresponding to the bipotent NC or the early neuronal progenitors. On the other hand, the more mature mouse neuronal progenitors (mouse c3 and c4) showed higher similarity with the human C6 and C8, the cells obtained from day 20 of differentiation, suggesting that the 20 day-differentiation of hNC can give rise to various neuronal progenitors resembling the developing ENS in E13.5 mouse embryonic gut. The cells collected from day 40 of differentiation (C8–C12) were more heterogeneous (Figure 1B) and contained various enteric neuronal subtypes (*NOS1*, *ADCYAP1*, *HTR2B*, *HTR3B*, *CALCB*, *NPY*, *CCK*, and *TH*) co-expressing a panel of associated transcription factors (TFs)²⁶ (Figure 1E). Importantly, a highly comparable expression dynamics was observed along the pseudotime development of human and mouse NC, where the neuronal (*TUBB3*, *ELVAL3*, *TH*, and *ADCYAP1*) genes were gradually up-regulated, accompanied by the down-regulation of the glial genes (*SOX10* and *FABP7*) (Figure 1F). These data strongly suggest that the mouse and human enteric NCs likely share similar molecular mechanisms underlying the neural fate acquisition. Therefore, understanding the molecular control of the neuronal lineage differentiation of NC in mice will help improve the differentiation protocol to generate hNC of greater neurogenic potential.

Transient Activation of Various Hedgehog Pathway Genes in Mouse Enteric Neural Crest

Transcriptional output of hedgehog signaling is governed by the combinatorial action of GLI1, GLI2, and GLI3. The mouse reporter line *Tg(GBS-GFP)*, in which GFP expression is driven by GLI TFs that bind to the 8 concatenated GLI-binding sequence (GBS),¹⁵ allows the *in vivo* monitoring of GLI activity (a readout of hedgehog signaling) in the enteric NC. As shown in Figure 2A, GFP signal was detected in the gut mesenchyme (adjacent to the epithelium) and in a small population of enteric NCs in the E11.5 *Tg(GBS-GFP)* embryonic guts. When hedgehog signal was activated by knocking out *Ptch-1* (a negative regulator of hedgehog signaling), the GFP signal in the gut mesenchyme and enteric NCs was increased, which was not limited to the intensity of GFP signal in enteric NCs but also included the number of GFP⁺ enteric NCs (Figure 2B). Consistently, overexpressing the repressor form of Gli3 (Gli3^{Δ699/Δ699}) inhibited hedgehog signaling, resulting in switching off the GFP signal in the gut mesenchyme and enteric NCs (Figure 2A, lower panel). These data emphasized



the specificity of the GFP signal in this reporter line. Then, we used this reporter line to study the dynamic of hedgehog signaling along the neuronal lineage differentiation trajectory of the enteric NC. By FACS (Figure 2C), we found that, in E13.5 guts, approximately $17.5\% \pm 0.6\%$ of cells are NC ($p75^{\text{NTR}+}$, $n = 6$), whereas only $11.9\% \pm 0.7\%$ are positive for GFP (Hh^{ON} ; $n = 10$). The transcriptional profiles of 2017 Hh^{ON} and 1841 Hh^{low} $p75^{\text{NTR}+}$ cells (Hh^{OFF} in Figure 2A) from E13.5 *Tg(GBS-GFP)* guts were quantified (Supplementary Figure 1). We used t-distributed stochastic neighbor embedding to visualize gene expression dynamics of these Hh^{ON} and Hh^{low} $p75^{\text{NTR}+}$ cells and overlaid them with the 7671 YFP⁺ cells isolated from E13.5 *Wnt-cre;YFP* guts (Figure 2D). Both the Hh^{ON} and Hh^{OFF} cells were distributed in all 8 clusters, corresponding to various cell states along the neuronal and glial lineage differentiation trajectories (Figure 2D), suggesting that GLI activity changes dynamically along the enteric NC cell progression. To investigate how these genes may contribute to the cell-state progression, we examined their expression levels in different clusters of the Hh^{ON} and Hh^{OFF} populations. Importantly, the expression levels of *Ptch1*, *Gli3*, and *Sufu* were elevated in the BP population of the Hh^{ON} population (\log_2 fold change > 1) and before the enteric NC transited from the bipotent state to the neuronal fate (Figure 2E). *Ptch1* and *Sufu* are negative regulators of the hedgehog pathway, and as direct GLI target genes, their expression is activated by hedgehog signaling. On the other hand, although *Gli3* encodes the major repressor of the hedgehog pathway, the full length form of GLI3 can function as an activator. These observations suggest a potential involvement of hedgehog signaling in the cell-state transition of enteric NC.

To validate these observations, we performed immunohistochemical analysis of embryonic guts at E11.5–E14.5 with GFP and various differentiation markers. At E11.5, GFP signals were detected in the progenitor populations, mainly in mBP ($\text{Sox10}^+\text{Phox2b}^+\text{Tuj1}^+$) (Figure 2F, filled arrowheads), whereas low levels of GFP could also be observed in some mGP ($\text{Sox10}^+\text{Phox2b}^-$) (Figure 2F, open arrowheads). Nevertheless, GFP signal was not found in the fully differentiated cells expressing high levels of Tubb3 (Tubb3^{high}) or other late-stage neuronal (Elavl4) and glial markers (Fabp7) in E14.5 guts (data not shown). Next, we examined how alterations of hedgehog pathway activity affect the cell-state transition of enteric NC in mice. The hedgehog pathway was activated in mice by the deletion of *Ptch1* (*bIII3a-Cre;Ptch1^{fl/fl}*) or *Sufu* (*Wnt1-Cre;Sufu^{fl/fl}*) as well as suppressed by the constitutive expression of a truncated GLI3 repressor in *Gli3^{Δ699/Δ699}* mice. As these mutants died on or before E13, as described previously,^{5,8} E12.5 guts were collected and the BP, neuronal progenitor, and GP were identified

based on the expression of Sox10, Phox2b, and/or Tubb3 (Tuj1). In addition to an early emergence of the mGP (Figure 2G, open arrowheads) in the *Ptch1* and *Sufu* mutant guts as described previously,^{5,8} we found that the mNP_{late} (Figure 2G, dark pink arrowheads) neuronal progenitor populations are increased with concomitant reductions of the mNP_{early} (Figure 2G, light pink arrowheads) and mBP (Figure 2G, white arrows) cells in both *Ptch1* and *Sufu* mutants (Figure 2G). Conversely, constitutive suppression of the hedgehog pathway significantly increased the mBP population and reduced the number of mGP cells in *Gli3^{Δ699/Δ699}* mice (Figure 2G). Taken together, these data suggest that hedgehog pathway activation promotes the progression of bipotent enteric NCs to differentiate into more mature cell states.

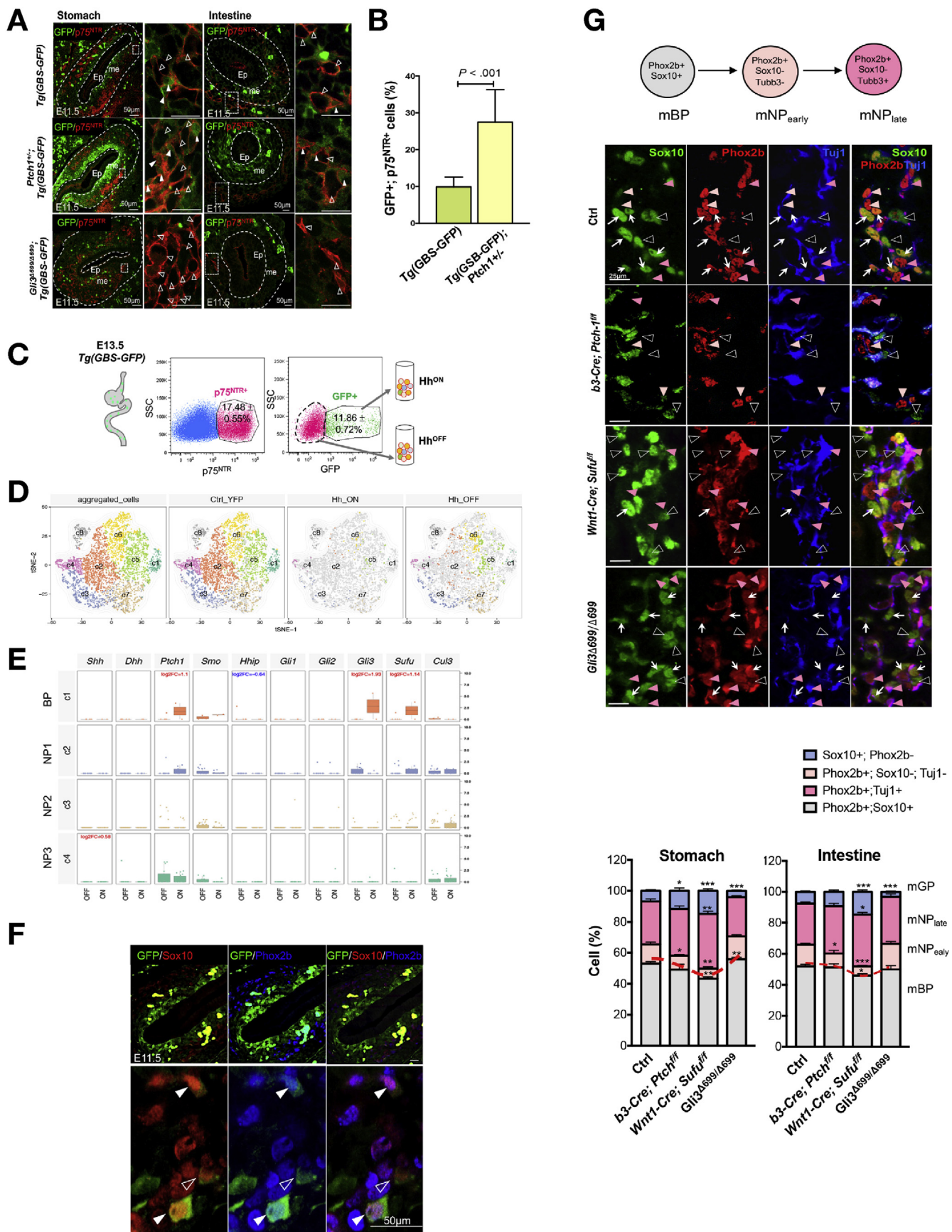
Level of Hedgehog Signaling Determines Neural Crest Yield From Human Pluripotent Stem Cells

To determine whether manipulation of hedgehog signaling could promote the cell-state transition and favor the generation of more mature NC of greater neurogenic potential from hPSC-derived cells, we used a pharmacologic approach to alter hedgehog pathway activity at the early and/or late phases of the hPSC differentiation process. An SMO agonist (SAG) and antagonist (cyclopamine) were added for various time frames during hPSC differentiation to activate and suppress hedgehog signaling, respectively (Figure 3A and D). Addition of SAG throughout the whole differentiation process (days 0–10, constant) significantly increased the yield of HNK-1⁺ $p75^{\text{NTR}+}$ cells (hNCs) as detected by flow cytometry. Intriguingly, the SAG incubation time could be shortened to as little as 4 days. If SAG was added for 4 days in the early phase (days 0–4) of the hPSC differentiation process, the NC yield was comparable to that in the 10-day SAG group (Figure 3B and C). Conversely, addition of cyclopamine during the early phase of hPSC differentiation dramatically suppressed the hPSC-to-NC transition, as evidenced by the reduced percentage of hNC (Figure 3E and F). These results indicate that hedgehog signaling is critical during the early phase of the hPSC-to-NC transition. A high level of hedgehog signaling in the early phase of the NC derivation from hPSC favors the hPSC-to-NC transition and promotes the generation of hNC cells, whereas inhibition of the hedgehog pathway abrogates this process.

Smoothed Agonist Primes Neural Crest Toward the Neurogenic Lineage

To understand how hedgehog signaling influences the topology of the neuronal differentiation path of hNC, we profiled another 768 single-cell transcriptomes of hNC cells

Figure 1. Single-cell RNA-seq showed the differentiation trajectories of human and mouse enteric NC. (A) Derivation of hNCs and hNPs from hPSCs. (B, C) PCA mapping of single-cell expression profiles of (B) human and (C) mouse enteric NC and their derivatives. (D) Density plot and Spearman correlation analysis of human and mouse enteric NC along the pseudotime development. (E) Expression of the enteric neuronal subtype markers and the associated transcription factors. (F) Expression of the selected stage-specific markers in human and mouse enteric NC at the indicated cell stage. D, day.



with constant (days 0–10) or early-phase (days 0–4) SAG stimulation and 384 early neuronal progenitors derived from hNC^{SAG0-10}, as shown in **Figure 4A**. Together with 2342 hNC and their derivatives, a total of 3494 individual cells were sequenced (**Supplementary Figure 1**). We then projected all single cells on the PCA plots to examine how the SAG may affect the topology of NC differentiation. The differentiation trajectory begins with the hNC (*SNAI1*⁺, *SOX10*⁺), passes through the early neuronal intermediates (hNP-D20; *TUBB3*^{high}, *ELAVL4*⁺), and terminates at a mature neuron state (hNP-D40; *TUBB3*^{high}, *ELAVL4*⁺) (**Figure 4B** and **C**). The addition of SAG for 4 days and 10 days during the NC induction consistently primed hNC (hNC^{SAG0-4} and hNC^{SAG0-10}) to the neurogenic fate. The hNC from the SAG groups stayed at the beginning of the differentiation trajectory as inferred by PCA analysis, but these cells already expressed a neurogenic marker (eg, *TUBB3*) (**Figure 4B** and **C**). Importantly, the neurons derived from these cells (hNC^{SAG0-10}-D20) were more mature than the untreated group with transcriptional profiles closer to the late neuronal progenitors (hNP-D40) (**Figure 4B** and **D**). All of these data suggest that SAG primes hNC toward the neurogenic lineage and favors the hNC-to-neuron transition.

We further analyzed the molecular dynamics during the early hNC-to-neuron transition in the presence or absence of SAG. We first clustered hNC and hNP-D20 into 8 clusters according to their transcription profiles and then divided these clusters into 3 classes corresponding to the 3 major developmental stages (early, stage 1; intermediate, stage 2; and late, stage 3) inferred by the pseudotime analysis and analyzed the sequential changes of DEGs during the stage transitions (**Supplementary Figure 3**). Stage 1 involved the down-regulation of genes implicated in “NC differentiation/development,” “PI3K-Akt signaling,” and “extracellular matrix receptor interaction.” It was followed by the up-regulation of genes mediating “cell fate commitment,” “Notch signaling pathway,” and “autonomic nervous system development” in stage 2, whereas the genes implicated in axon development were up-regulated during the transition to the final stage (**Figure 4E**, **Supplementary Figure 4**, and **Supplementary Table 3**). The 2 SAG-specific NC intermediates that emerged during the stage 1-to-stage 2 transition exhibited unique gene expression profiles with predominant involvement in the Gene Ontology term “metabolism-related pathways” (**Supplementary Figure 5**). We then focused on TFs

differentially expressed in progressive cell fate transition from NC to neuron and constructed the gene network based on their pairwise correlations. Three subnetworks were shown chronologically, in which most of stage 2 and some of stage 3 TFs were up-regulated by SAG (**Figure 4F**, *yellow circles*). In particular, many of the stage 2 TFs, including *INSM1*, *NHLH1*, and other bHLH family members (*NEUROD*), are the known direct targets of *GLI2*.²⁷ These stage 2 transcription drivers also connected with genes in stage 3, implying that the SAG activates the transcriptional circuits for initiating cell commitment/differentiation, priming NC toward the neurogenic lineage.

Smoothed Agonist Favors Neural Crest Derivation From Human Pluripotent Stem Cells at Various Steps of Differentiation

To explore how SAG influences various steps of the NC derivation from hPSCs and their subsequent neuronal lineage differentiation, we performed the experiments illustrated in **Figure 5A**. During the early phase of NC induction, a brief activation of the hedgehog pathway (2 days) could significantly enhance the ectoderm lineage commitment of hPSC, increasing the number of *SOX2*⁺*NANOG*⁻ cells at day 4 of differentiation (**Figure 5A** and **B**). However, longer incubation with SAG (4 days) will be needed to induce the robust formation of *SNAI1*⁺ NC-like cells (**Figure 5A** and **C**). Nevertheless, prolonged (days 0–10) or late-phase (days 4–10) incubation with SAG indeed boosted the NC-to-neuron transition. As shown in **Figure 5D** and **E**, the hNC, hNC^{SAG0-10}, and hNC^{SAG4-10} cells could give rise to comparable numbers of neurons expressing various pan-neuronal markers (HU, TUJ1, and protein gene product [PGP] 9.5). On the other hand, hNC^{SAG0-10} and hNC^{SAG4-10} cells exhibited better differentiation competency and required a shorter differentiation time to generate neuronal subtypes, such as tyrosine hydroxylase (TH) and vasoactive intestinal polypeptide (VIP)-expressing neurons. Significantly larger numbers of TH⁺ and VIP⁺ neurons were obtained from NC^{SAG0-10} cells at day 22 of differentiation when compared with the control (**Figure 5D**). In the control group, numbers of TH⁺ and VIP⁺ neurons comparable to those in the SAG group at day 22 were observed only on day 32 of differentiation, as described previously.¹ Thus, SAG favors cell-state transition along the hPSC-to-NC-to-neuron differentiation trajectory.

Figure 2. Dynamic activation of hedgehog signaling in the developing ENS. (A) Immunohistochemistry on *Tg(GBS-GFP)* embryonic guts with wild-type, *Ptch1*^{+/−}, and *Gli3*^{4699/4699} background. Open and filled arrowheads mark GFP-negative (GFP[−]) and positive (GFP⁺) enteric NCs, respectively. (B) Flow analysis of the percentage of GFP⁺ enteric NCs in E11.5 control and *Ptch1* mutant guts. (C) Scheme of isolation of GFP⁺ (*Hh*^{ON}) and GFP[−] (*Hh*^{OFF}) enteric NC from E13.5 *Tg(GBS-GFP)* embryonic guts using FACS. (D) t-SNE projection of 7671 YFP⁺, 2017 *Hh*^{ON}, and 1841 *Hh*^{low} enteric NCs, colored by the indicated cell types. (E) Boxplots show the expression of hedgehog pathway genes in different clusters of *Hh*^{ON} and *Hh*^{OFF} enteric NC. (F) Immunohistochemistry on *Tg(GBS-GFP)* embryonic guts at E11.5 for detection of bipotent (BP; *Phox2b*⁺*Sox10*⁺); neuronal (NP; *Phox2b*⁺*Sox10*[−]); glial (GP; *Phox2b*[−]*Sox10*⁺), and GFP signal. (G) Scheme of cell-state transition along the neuronal differentiation of enteric NC in mouse. Immunohistochemistry for the detection of various progenitors in the stomach and intestine of E12.5 control, *Ptch1* (*b3-IIIa-Cre*; *Ptch1*^{fl/fl}), *Sufu* (*Wnt1-Cre*; *Sufu*^{fl/fl}), and *Gli3* (*Gli3*^{4699/4699}) mutants. Bar chart shows the quantitative data. Ctrl, control; Hh, hedgehog; t-SNE, t-distributed stochastic neighbor embedding; YFP, yellow fluorescent protein.

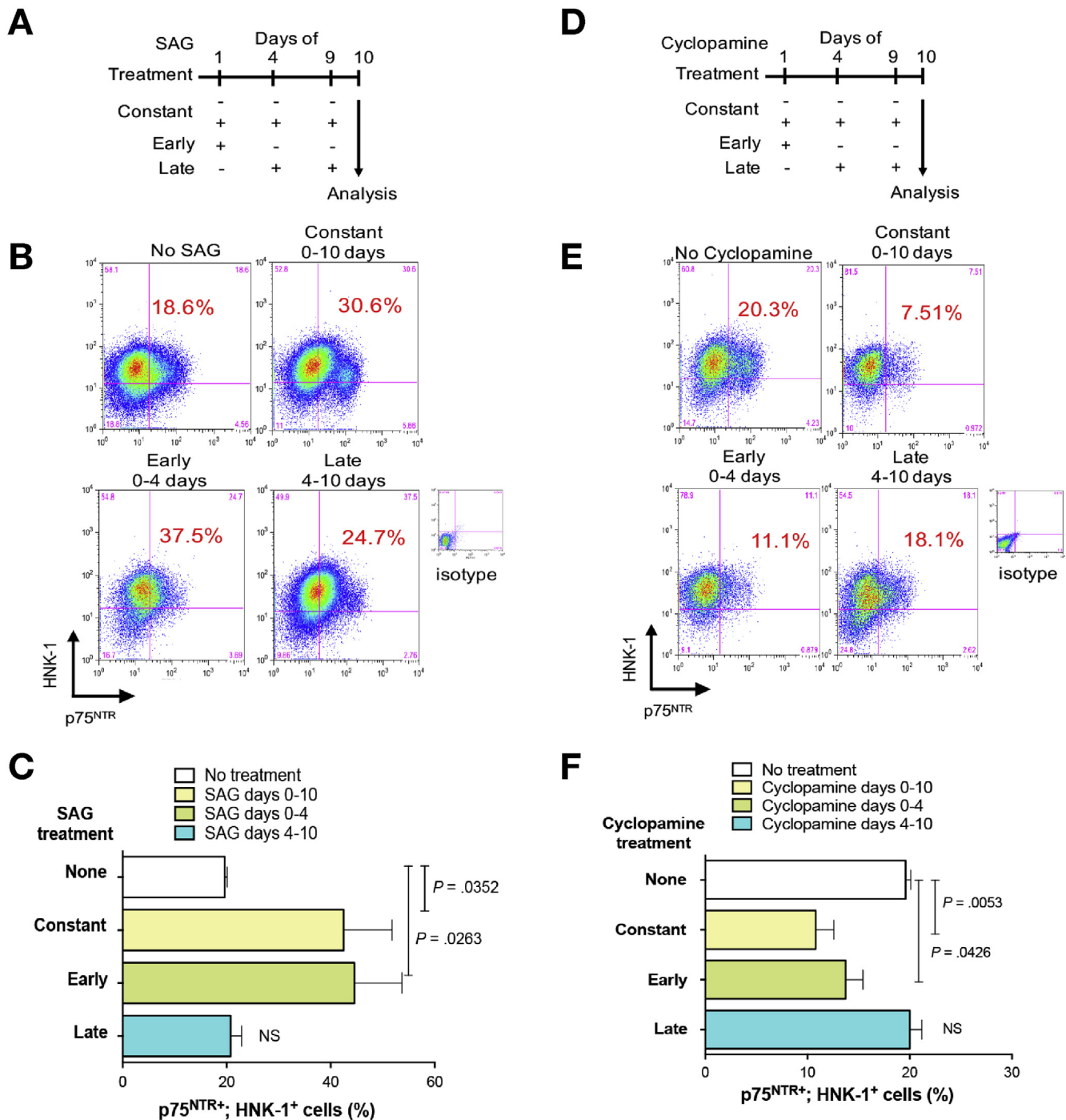


Figure 3. Level of hedgehog signaling affects the hPSC-to-NC transition. (A, D) Schemes of NC differentiation in the presence of SAG or cyclopamine. Flow analysis of HNK-1⁺p75^{NTR}⁺ cells at day 10 of NC derivation from hPSC after incubation with (B) SAG and (E) cyclopamine. (C, F) Bar charts summarize the percentages of HNK-1⁺p75^{NTR}⁺ cells in 3 independent experiments.

Establishment of an Innervated Colonic Organoid Model Comprising Functional Neurons

Next, we established an innervated HCO model for appraising the functional competency of hNC cells derived from our new SAG protocol. Hereafter, the hNC cells used for the generation of the innervated HCOs will be termed ENCCs. In brief, our organoid model comprises 2 major components: ENCCs and gut endodermal cells. As shown in Figure 6A, the ACTIVIN-NODAL and WNT pathways were

activated sequentially to promote the formation of definitive endoderm and hindgut spheroids, respectively. On day 6, hPSCs had differentiated into definitive endoderm co-expressing SOX17 and FOXA2 (Figure 6B). The free-floating spheroids derived from the definitive endoderm were collected on days 8–10 and cultured with the FACS-sorted ENCCs in 3-dimensional Matrigel, in which ENCCs received patterning signals from the gut endoderm and developed together with the endodermal cells. The hindgut

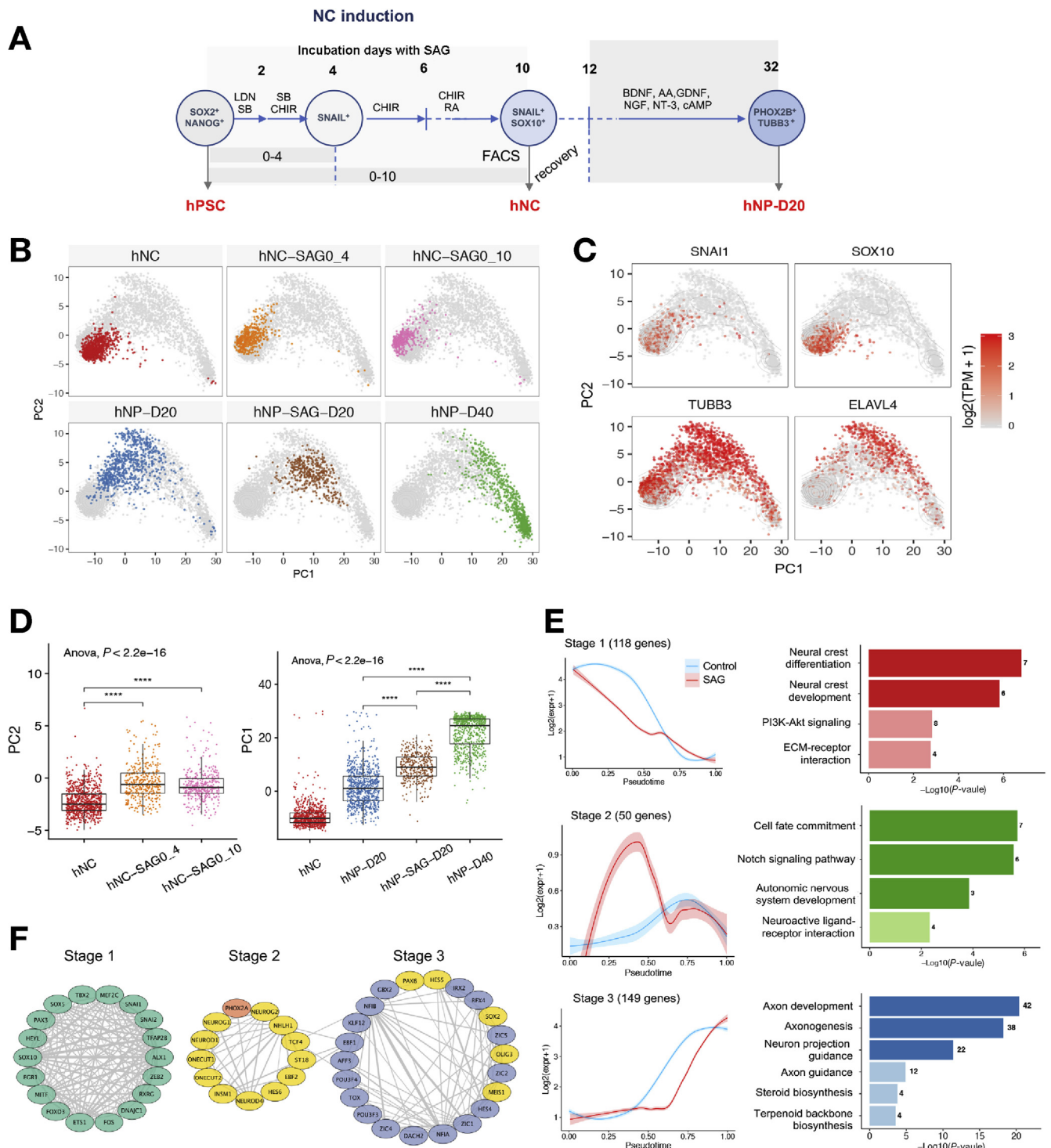


Figure 4. High-resolution dissection of NC-to-neuron transition using scRNA-seq. (A) Scheme of the derivation of hNC and hNP from hPSC. (B) PCA visualization of all 3494 individual cells during the whole differentiation process, colored by the indicated cell types. (C) Expression of NC (*SNAI1*, *SOX10*) and neuronal (*TUBB3*, *ELAVL4*) marker genes along the hNC-to-neuron differentiation path confirms cell fate progression toward the neuronal lineage. (D) PC scores of hNC and hNP in control and SAG groups. (E) The expression dynamics of 425 top DEGs were cataloged into 3 major groups in a pseudotime manner, shown as blue lines (control) and red lines (SAG group). Thick lines indicate the average gene expression patterns in each group. Gene Ontology (dark-colored bars) and Kyoto Encyclopedia of Genes and Genomes pathway (light-colored bars) analyses of each gene group. (F) Gene correlation network during NC-to-neuron transition. Green, orange, and blue colors represent the key TFs uniquely expressed in each stage. Yellow represents the TFs that are up-regulated in the SAG groups.

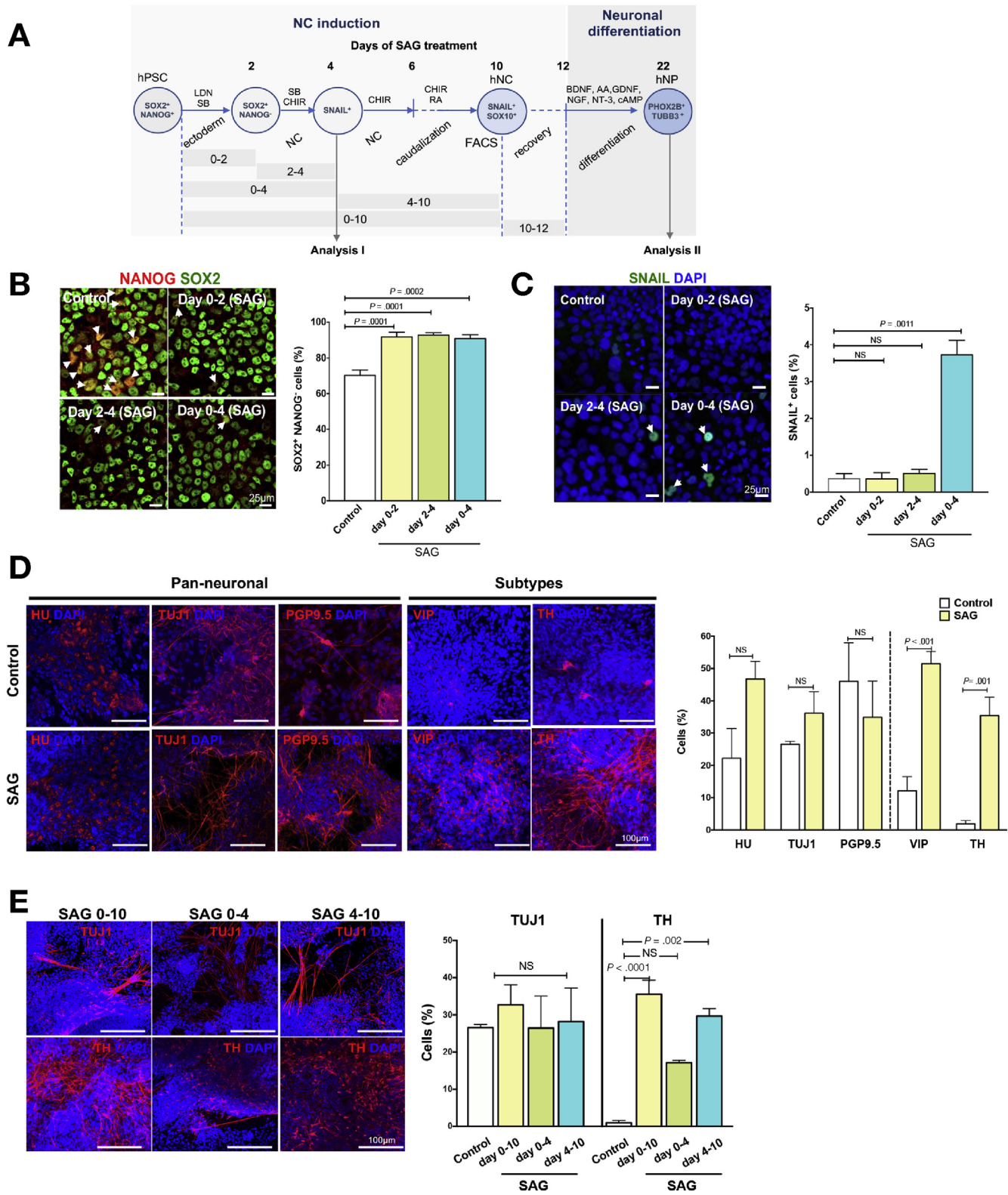
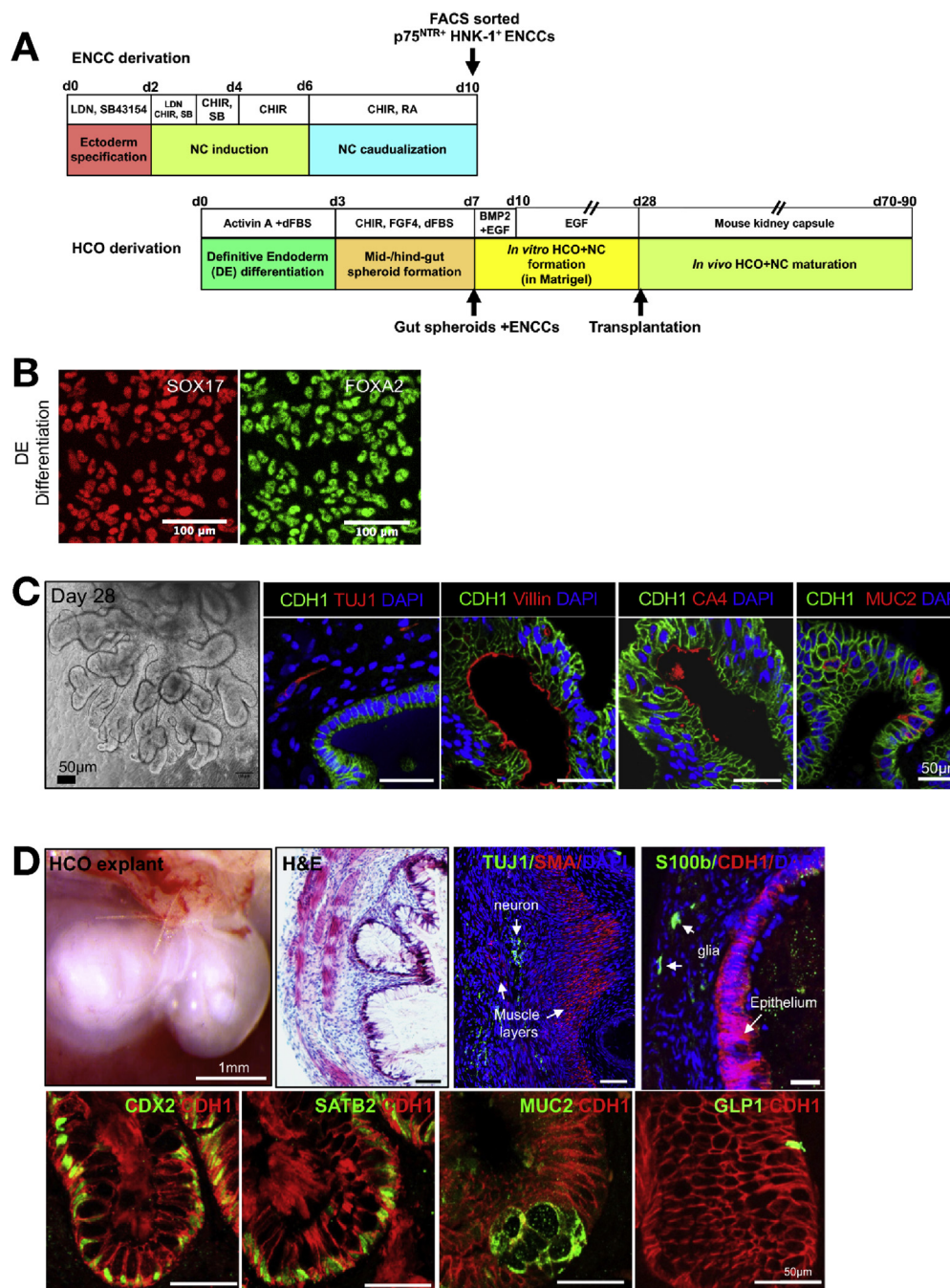


Figure 5. SAG promotes derivation of hNCs from hPSCs and enhances their neurogenic competency. (A) The addition of SAG at different phases of differentiation. (B) Ectoderm lineage differentiation was monitored by using immunocytochemistry (pluripotent stem cell: SOX2⁺NANOG⁺; ectoderm: SOX2⁺NANOG⁻). The bar chart shows the percentage of SOX2⁺NANOG⁻ cells in each group. (C) Immunocytochemistry was used to detect NC cells (SNAIL⁺). The bar chart shows the percentage of SNAIL⁺ NC cells in each group. (D, E) At day 22 of differentiation, control, hNC^{SAG0-10}, hNC^{SAG0-4}, and hNC^{SAG4-10} expressed various pan-neuronal markers (HU, TUJ1, and PGP9.5) and TH and VIP. The bar charts show the quantitative data.



spheroids were then caudalized further by the addition of BMP2 (Figure 6A). By day 28, the HCOs showed villus-like structures containing a distinct layer of gut epithelium (VILLIN⁺, CDH1⁺) expressing a colon-specific marker (CA4⁺) and goblet cells (MUC2⁺) (Figure 6C). Intriguingly, ENCCs showed the ability to self-pattern, align with the epithelium, and start differentiating into neurons (TUJ1⁺) (Figure 6C). After transplantation into the kidney capsule of immunodeficient mice, HCOs underwent morphogenesis and formed mature tissues with defined crypts and colonic epithelium, whereas ENCCs gave rise to nerve cells (TUJ1⁺ neurons and S100b⁺ glia) residing near the submucosal and myenteric layers of smooth muscle fibers (Figure 6D).

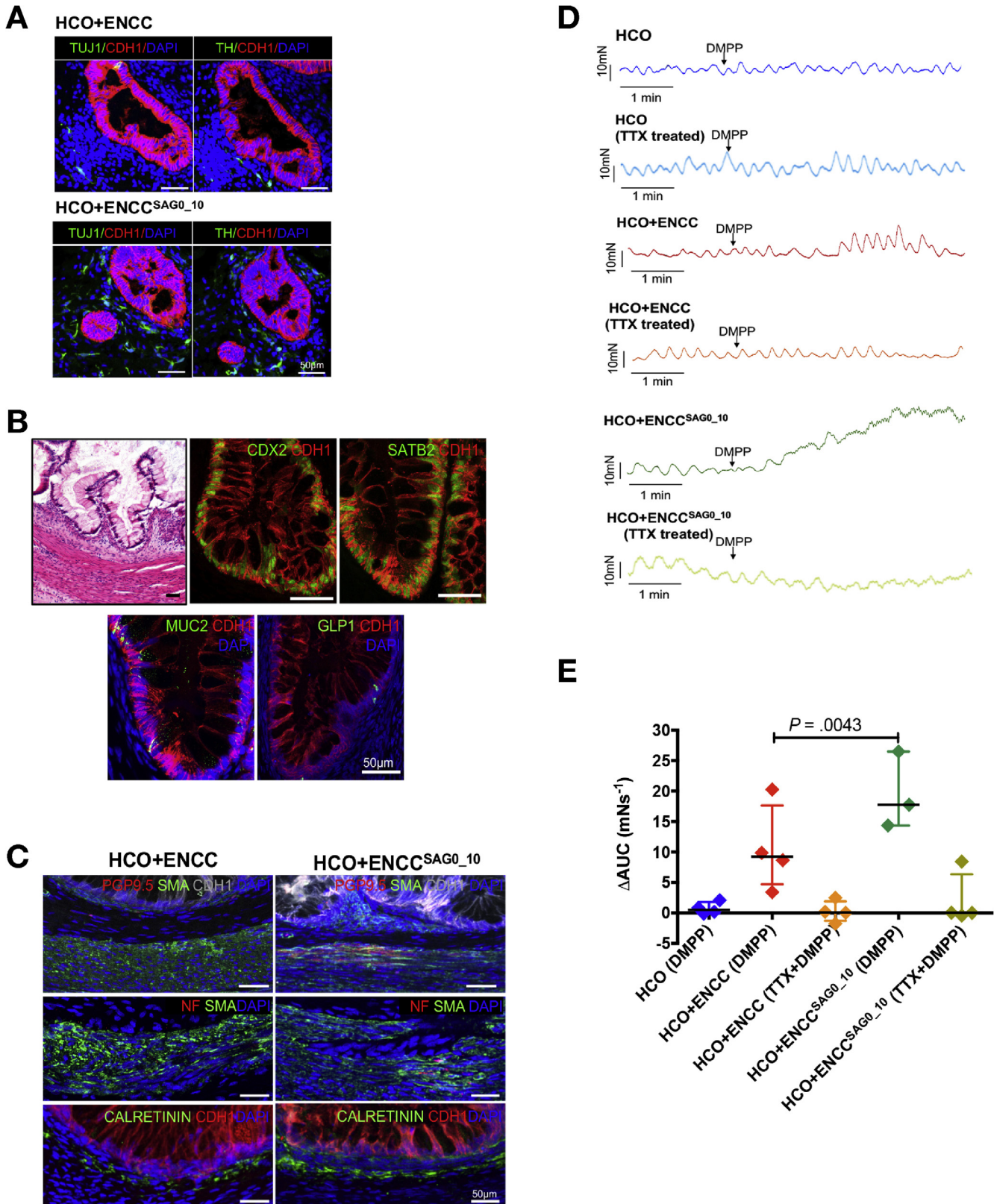
Consistently, expressions of gut epithelium (CDH1⁺) and colon (SATB2⁺) markers were detected, and goblet-(MUC2⁺) and endocrine-like cells (GLP1⁺) were found in the mature HCOs (Figure 6D).

Early Activation of Hedgehog Improves the Functional Competency of Enteric Neural Crest-Derived Neurons as Shown by the Innervated Human Colonic Organoid Model

We then examined the impact of SAG on the function of ENCC-derived neurons on the basis of inducing HCO contractions. Innervated HCOs were generated by using control

ENCCs and ENCCS^{SAG0-10}. Consistently, we found that ENCCS^{SAG0-10} grew better than the control ENCCs with HCOs in vitro, and more TUJ1⁺ and TH⁺ cells were found

aligned with the epithelial cells of HCOs in the SAG group (Figure 7A). The HCO plus ENCCS^{SAG0-10} explants contained crypts and colonic epithelium, highly comparable to that of



the control group (**Figure 7B**). Intriguingly, more mature neurons expressing PGP9.5 and neurofilament (NF) were detected in the SAG group, whereas the majority of neurons detected in the control group expressed only the neuronal progenitor marker TUJ1. On the other hand, calretinin-positive nerve cells were detected in all innervated HCO explants (HCO plus ENCCs and HCO plus ENCC^{SAG0-10}), suggesting that most NC-derived neurons are excitatory neurons (**Figure 7C**).

To examine the neuromuscular coupling mediated by the ENCC-derived neurons, we randomly dissected part of the HCO explants from each group for functional tests. Slow waves and rhythmic phasic contractions were found in all HCOs with or without ENCCs. These contractions were irregular in frequency, smaller in amplitude, and likely driven by interstitial cells of Cajal. We then activated the ENCC-derived neurons using the selective α 3-nicotinic receptor agonist dimethylphenylpiperazinium, which increases nerve excitability by inhibiting Na^+ channel inactivation. As illustrated in **Figure 7D**, dimethylphenylpiperazinium elicited a much greater muscle contraction in HCOs plus ENCCs, whereas only some irregular small waves of contractions were observed with HCOs lacking ENCCs. Muscle contraction was mediated by ENCC-derived neurons because the addition of tetrodotoxin completely abolished muscle contraction. In addition, stronger contractile responses were usually observed in the SAG-treated group (HCO plus ENCC^{SAG0-10}, **Figure 7D**). These results were reproducible across independent experiments and innervated HCOs derived from 2 different hPSC lines (**Figure 7E**). Overall, SAG greatly speeded up the maturation of ENCC-derived neurons and improved their functional competency.

Discussion

The limited yield and immature differentiation of hPSC derivatives remain the major challenges for applications in regenerative medicine. We have described a robust strategy for deriving NC from hPSCs by activating hedgehog signaling during NC induction. Together with our newly established innervated HCO model, we clearly showed that our approach significantly improves not only NC yield from hPSCs but also the differentiation capability of hPSC-derived NC to the neuronal lineage and the neuromuscular coupling of the neurons.

Lineage decision making is fundamentally a single-cell process, and the response to lineage-specifying signals depends on the state of the individual cell. Therefore, directed differentiation of hPSC usually gives rise to heterogeneous populations, resembling cells at various intermediate

differentiation states during development *in vivo*. Through understanding the molecular control of the cell-state transition using mouse models, we may further improve the differentiation protocol to generate more mature cells with better functional competency. High-resolution RNA-seq of mouse NC derivatives allows us to identify the unique expression profiles of these intermediate populations. By cross-referencing the known stage- and cell-fate-specific markers gleaned from the *in vivo* studies, the stereotypical sequence of these intermediate states and the developmental trajectories of mouse NC can be established. In addition, the sequential molecular dynamics that direct mouse NC toward the neurogenic lineage can be depicted by building the pseudotime trend for the NC-to-neuron transition, such that the ordered activation of transcriptional waves throughout the trajectory of neuronal differentiation can be revealed. A better understanding of the decision-making process that underlies cell-state progression will help improve the existing differentiation protocol in a systematic way.

From this study, we provided evidence that after 20 days of neuronal differentiation, hNC cells give rise to neuronal progenitors resembling numerous neuronal intermediates found in the E13.5 mouse gut. The pseudotime analysis also suggested that human and mouse enteric NC cells share similar differentiation trajectories, emphasizing the feasibility of using hPSC-derived NC cells to replenish the missing neurons in aganglionic guts. The next important step is to define the molecular cues boosting the neurogenic differentiation of these cells. Mouse studies have suggested that hedgehog signaling is implicated in the early phase of enteric NC differentiation,^{5,8} but the underlying mechanism remains elusive. With the GBS-reporter line, we found that only 10%–13% of the enteric NCs exhibit high GLI activity during the early phase of the ENS development (E11.5–E14.5). Our single-cell transcriptomics data and immunohistochemistry analysis suggest that hedgehog pathway is likely activated in the BP population, whereas perturbing hedgehog signaling affects not only the pool size of the BP population but also that of the neuronal progenitor and GP populations in E12.5 mouse gut (**Figure 2F**). These data suggest that the activation of the hedgehog pathway likely promotes the cell-state transition instead of directing the enteric NC to a specific lineage. This notion is also supported by the subsequent transcriptomics analysis using an hPSC model. The molecular dynamics and network analyses suggest that at least 3 subsets of gene regulatory circuits are involved in mediating the NC-to-neuron transition, where the stage 2 and stage 3 subnetworks are interconnected. SAG, in particular, robustly up-regulated the key TFs

Figure 7. SAG improves the neuromuscular coupling of ENCC-derived neurons. (A) Immunocytochemistry analysis of day 28 HCOs showed more TUJ1⁺ and TH⁺ neurons in the SAG group. (B) H&E staining of colon tissue after transplantation. Detection of the expression of markers for colon (CDX2, SATB2), goblet (MUC2), and endocrine (GLP-1) cells in the HCO plus ENCC^{SAG0-10} explants. (C) Immunohistochemistry detects the expression of markers for mature (PGP9.5, NF) and excitatory (calretinin) neurons, epithelium (CDH1), and muscle layer (SMA). (D) HCOs (top), HCOs plus ENCCs (middle), and HCO plus ENCCs^{SAG0-10} (bottom) explants subjected to low-voltage electrical field stimulation (5-ms pulse at 30 V) in with or without TTX (10 $\mu\text{mol/L}$, 5 min). (E) Dimethylphenylpiperazinium (DMPP) stimulation in HCO, HCO plus ENCCs, and HCO plus SAG-ENCC^{SAG0-10} in the absence or presence of TTX.

implicated in these 2 interconnecting subnetworks, implying that the activation of the hedgehog pathway likely favors the stage 2-to-stage 3 transition and primes NC toward the neurogenic lineage (Figure 4G and H). In addition, metabolic pathways were robustly activated in the SAG groups, and the enhanced cellular metabolism may function as a booster in the NC-to-neuron transition, particularly favoring neurogenesis.

In this study, we also established a new differentiation protocol for generating innervated HCOs and used it to assess the functional competency of the hPSC-derived NC cells. It is a near-physiologic model in which NC cells lined up along the epithelial cells of HCOs, self-organized, and gave rise to the enteric neurons in response to inductive cues from the developing HCOs, recapitulating the gut morphogenesis process *in vivo*. We consistently found that many more TUJ1⁺ cells were detected in the HCO^{SAG} (Figure 7A), suggesting that SAG may improve the survival and/or engraftment efficiency of the ENCCs to HCOs. Consistent with our cell data, the HCO explants from the SAG group contained more mature enteric neurons (PGP9.5⁺ and NF⁺), and that led to the better contractile responses of the innervated HCOs than in the control group. Thus, the application of SAG represents a generic way to promote the cell-state transition, speed up the maturation of nerve cells, and make the differentiation protocol highly reproducible among independent experiments and across different hPSC lines.

In summary, we have established an experimental algorithm that provides guidance for more efficient ways to generate mature neurons from hPSC-derived NC. The scRNA-seq analysis showed that hedgehog signaling represents the differentiation cue associated with the transition from immature NC intermediates to the more mature cell-state and the priming of NC toward the neuronal lineage. Windows of opportunity have been identified at the early and late phases of the hPSC-to-NC-to-neuron transition, which can be exploited to guide NC lineage differentiation with maximal yield and functional competency, respectively. More importantly, our innervated HCO model represents an *in vitro* system closely resembling how a real gut functions. It has the potential to drive breakthroughs not only in mechanistic studies of various gastrointestinal diseases but also in drug development and toxicity tests.

Supplementary Material

Note: To access the supplementary material accompanying this article, visit the online version of *Gastroenterology* at www.gastrojournal.org, and at <https://doi.org/10.1053/j.gastro.2019.08.019>.

References

- Lai FP, Lau ST, Wong JK, et al. Correction of Hirschsprung-associated mutations in human induced pluripotent stem cells via clustered regularly interspaced short palindromic repeats/Cas9, restores neural crest cell function. *Gastroenterology* 2017;153:139–153.
- Lee G, Chambers SM, Tomishima MJ, et al. Derivation of neural crest cells from human pluripotent stem cells. *Nat Protoc* 2010;5:688–701.
- Menendez L, Kulik MJ, Page AT, et al. Directed differentiation of human pluripotent cells to neural crest stem cells. *Nat Protoc* 2013;8:203–212.
- Fattah F, Steinbeck JA, Kriks S, et al. Deriving human ENS lineages for cell therapy and drug discovery in Hirschsprung disease. *Nature* 2016;531(7592):105–109.
- Liu JA, Lai FP, Gui HS, et al. Identification of *GLI* mutations in patients with Hirschsprung disease that disrupt enteric nervous system development in mice. *Gastroenterology* 2015;149:1837–1848.
- Munera JO, Sundaram N, Rankin SA, et al. Differentiation of human pluripotent stem cells into colonic organoids via transient activation of BMP signaling. *Cell Stem Cell* 2017;21:51–64.
- Li XJ, Du ZW, Zarnowska ED, et al. Specification of motoneurons from human embryonic stem cells. *Nat Biotechnol* 2005;23:215–221.
- Ngan ES, Garcia-Barcelo MM, Yip BH, et al. Hedgehog/Notch-induced premature gliogenesis represents a new disease mechanism for Hirschsprung disease in mice and humans. *J Clin Invest* 2011;121:3467–3478.
- Semrau S, Goldmann JE, Soumillon M, et al. Dynamics of lineage commitment revealed by single-cell transcriptomics of differentiating embryonic stem cells. *Nat Commun* 2017;8:1096.
- Cao J, Spielmann M, Qiu X, et al. The single-cell transcriptional landscape of mammalian organogenesis. *Nature* 2019;566(7745):496–502.
- La Manno G, Soldatov R, Zeisel A, et al. RNA velocity of single cells. *Nature* 2018;560(7719):494–498.
- Pijuan-Sala B, Griffiths JA, Guibentif C, et al. A single-cell molecular map of mouse gastrulation and early organogenesis. *Nature* 2019;566:490–495.
- Sauka-Spengler T, Bronner M. Snapshot: neural crest. *Cell* 2010;143:486.
- Workman MJ, Mahe MM, Trisno S, et al. Engineered human pluripotent-stem-cell-derived intestinal tissues with a functional enteric nervous system. *Nat Med* 2017;23:49–59.
- Balaskas N, Ribeiro A, Panovska J, et al. Gene regulatory logic for reading the Sonic Hedgehog signaling gradient in the vertebrate neural tube. *Cell* 2012;148:273–284.
- Böse J, Grotewold L, Rüther U. Pallister-Hall syndrome phenotype in mice mutant for *Gl3*. *Hum Mol Genet* 2002;11:1129–1135.
- Chen MH, Wilson CW, Li YJ, et al. Cilium-independent regulation of Gli protein function by Sufu in Hedgehog signaling is evolutionarily conserved. *Genes Dev* 2009;23:1910–1928.
- Ellis T, Smyth I, Riley E, et al. Patched 1 conditional null allele in mice. *Genesis* 2003;36:158–161.

19. Xue Y, Cai X, Wang L, et al. Generating a non-integrating human induced pluripotent stem cell bank from urine-derived cells. *PLoS One* 2013;8(8):e70573.
20. Tang CS, Li P, Lai FP, et al. Identification of genes associated with Hirschsprung disease, based on whole-genome sequence analysis, and potential effects on enteric nervous system development. *Gastroenterology* 2018;155:1908–1922.
21. Weinreb C, Wolock S, Klein AM. SPRING: a kinetic interface for visualizing high dimensional single-cell expression data. *Bioinformatics* 2018;34:1246–1248.
22. Kharchenko PV, Silberstein L, Scadden DT. Bayesian approach to single-cell differential expression analysis. *Nat Methods* 2014;11:740–742.
23. Yu G, Wang LG, Han Y, et al. clusterProfiler: an R package for comparing biological themes among gene clusters. *OMICS* 2012;16:284–287.
24. Lasrado R, Boesmans W, Kleinjung J, et al. Lineage-dependent spatial and functional organization of the mammalian enteric nervous system. *Science* 2017;356(6339):722–726.
25. Morrison JA, McLennan R, Wolfe LA, et al. Single-cell transcriptome analysis of avian neural crest migration reveals signatures of invasion and molecular transitions. *eLife* 2017;6:e28415.
26. Memic F, Knoflach V, Morarach K, et al. Transcription and signaling regulators in developing neuronal subtypes of mouse and human enteric nervous system. *Gastroenterology* 2018;154:624–636.
27. Yin WC, Satkunendran T, Mo R, et al. Dual regulatory functions of SUFU and targetome of GLI2 in SHH subgroup medulloblastoma. *Dev Cell* 2019;48:167–183.

Author names in bold designate shared co-first authorship.

Received April 16, 2019. Accepted August 14, 2019.

Reprint requests

Address requests for reprints to: Elly Sau-Wai Ngan, PhD, Department of Surgery, The University of Hong Kong, Faculty of Medicine Building, 21 Sassoon Road, Pokfulam, Hong Kong, SAR, China. e-mail: engan@hku.hk; fax: (852) 3917-9621.

Acknowledgments

The authors would like to thank James Briscoe (Francis Crick Institute, London, UK) for the *Tg(GSB-GFP)* reporter mouse line. Confocal imaging and scRNA-seq were performed, respectively, with equipment maintained by Li Ka Shing Faculty of Medicine Faculty Core Facility and Center for Genomic Sciences, University of Hong Kong.

Author contributions: Sin-Ting Lau, Frank Pui-Ling Lai, and Kathy Nga-Chu Lui analyzed hPSC-derived NC cells and NCOs. Frank Pui-Ling Lai performed genome editing on hiPSCs. Zhixin Li performed bioinformatics analyses. Guangjin Pan provided the control hPSC line. Jorge O. Munera, Maxime M. Mahe, and James M. Wells provided support for the organoid studies. Chi-Chung Hui provided transgenic mice for *in vivo* studies. Elly Sau-Wai Ngan supervised the project and prepared the manuscript.

Conflicts of interest

The authors disclose no conflicts.

Funding

This work was supported by an HMRF grant (project nos. 03143236, 06173306); a seed funding from Li Dak Sum Research Centre, the University of Hong Kong; and research grants from the Research Grants Council of Hong Kong Special Administrative Region, China Hong Kong (HKU17109215, HKU17112416) to Elly Sau-Wai Ngan.

Supplementary Methods

Mice

Tg(GBS-GFP), *Sufu*^{f/f}, *Gli3*^{A699}, *Ptch1*^{f/f}, *b3-IIIa-Cre*, and *Wnt1-Cre* mice were previously generated.^{1–5} Mice were maintained in a mix outbred background of C57 and 129/S6. Genotyping was performed with the primers listed in **Supplementary Table 1**. NOD/SCID mice were purchased from our animal unit. Animals were maintained in the Animal Laboratory at the Department of Surgery, University of Hong Kong. All experiments were performed in accordance with procedures approved by the committee on the Use of Live Animals, University of Hong Kong (CULTRA 2827-15, 3837-15, and 4181-16).

Human Induced Pluripotent Stem Cells

A control hiPSC line (IMR90-iPSC) was obtained from WiCell Research Resources (Wicell, WI, RRID:CVCL C434). Another control hiPSC cell line (UE02302) was generated from urine-derived cells of a male individual by episomal reprogramming vectors carrying the 4 reprogramming factors.⁶ All hiPSCs used in this study were at the intermediate (35–65) passage numbers and maintained on a Matrigel-coated (BD Biosciences, 354234) plate with mTeSR1 medium (StemCell Technologies, 05850).

Derivation of Neural Crest From Human Pluripotent Stem Cell Lines

At day 0, control or mutant hiPSCs were seeded on a Matrigel-coated plate (10^5 cells/cm²) in induced pluripotent stem cell medium containing 10 ng/mL fibroblast growth factor (FGF) 2 (PeproTech, Rocky Hill, NJ; 100-18B) and 10 μ mol/L Y-27632. Differentiation was then initiated by replacing iPS cell medium with knockout serum replacement medium, containing knockout Dulbecco's modified Eagle medium (DMEM) plus 15% KSR (Life Technologies, Rockville, MD; 10828-028), NEAA (Life Technologies, 11140-050), L-glutamine (Life Technologies, 25030-081), β -mercaptoethanol (Life Technologies, 21985-023), LDN193189 (100 nmol/L; Stemgent, Cambridge, MA), and SB431542 (10 μ mol/L; Tocris, Minneapolis, MN). The dual SMAD inhibitors and a potent GSK inhibitor were added at different time frames during the NC induction, including LDN193189 (from day 0 to day 3), SB431542 (from day 0 to day 4), and 3 μ mol/L CHIR99021 (from day 2 to day 10; Tocris, 4423). The NC cells were finally caudalized with 1 μ mol/L retinoic acid (from day 6 to day 9). The KSR medium was gradually changed to N2 medium at day 4 by increasing N2 from 25% to 75% from day 4 to 9, as described previously.⁷ The N2 medium contained neural basal medium (Life Technologies, 22103-049) and DMEM/F12 (Life Technologies, 10565-018 [1:1]), N2 supplement (Life Technologies, 17502-048), B27 supplement (Life Technologies, 17504-044) and insulin (Life Technologies, 12585-014). SAG (1 μ mol/L; Sigma-Aldrich, St Louis, MO; SML1314) or cyclopamine-KAAD (1 μ mol/L; Abcam, Cambridge, UK; ab142146) was added at the early (days 0–4) or

late (days 4–10) phases or constantly (day 0–10) during the in vitro differentiation. The NC cells were enriched by FACS with antibodies against p75^{NTR} and HNK-1 at day 10 of the differentiation, as described.^{7–11}

In Vitro Differentiation of Enteric Neural Crest-Derived Cells to Enteric Nervous System Neurons

Approximately 40,000 FACS-enriched NC cells were seeded as droplets on poly-ornithine/laminin/fibronectin-coated 24-well plates in N2 medium containing 10 ng/mL FGF2, 3 μ mol/L CHIR99021, and 10 μ mol/L Y-27632. The neuronal differentiation started 48 hours later, and the attached NC cells were then cultured with N2 medium containing brain-derived neurotrophic factor (10 ng/mL; PeproTech, 450-01), glial-cell derived neurotrophic factor (10 ng/mL; PeproTech, 450-10), and ascorbic acid (200 μ mol/L; Sigma-Aldrich, A4034-100G), neurotrophin-3 (10 ng/mL; PeproTech, 450-03), nerve growth factor (10 ng/mL; PeproTech, 450-01), and adenosine 3',5'-cyclic monophosphate (1 μ mol/L; Sigma-Aldrich, D0260). The culture medium was changed every 2 days. NC-derived neurons at differentiation day 9 were fixed for immunocytochemistry analyses, and neurons at days 20 (hNP-20) and 40 (hNP-40) were harvested by using Accutase for single-cell RNA sequencing.

Fluorescence-Activated Cell Sorting and Flow Cytometric Analysis

For mouse enteric NCs, guts were isolated from E13.5 *Wnt1-Cre*; *YFP* and *Tg(GBS-GFP)* embryos and digested with dispase/collagenase (0.2 mg/mL each, 37°C for 5 minutes). Cells were then resuspended in phosphate-buffered saline (PBS) with 2% fetal bovine serum (FBS) and passed through a 40- μ m cell strainer. The cells were incubated with p75^{NTR} (1:100 dilution, Abcam) and then phycoerythrin (PE)-conjugated anti-rabbit secondary antibody for detection. Labeled enteric NCs were detected with a BD FACSAria III Cell Sorter. PE and GFP double-positive cells were gated and sorted by using the 4-way purity mode. The purity of sorted cells was evaluated by flow cytometry and was >96%. Isotype-matched antibodies were used as controls. FlowJo, version 8.2 (Tree Star, Ashland, OR), was used to analyze flow data. The FACS-sorted cells were then subjected to scRNA-seq by using the 10 \times Genomics platform.

For quantifying the hNCs, the 10-day-differentiated cells were dissociated with Accutase and then incubated with anti-human antibodies, including APC-HNK-1 (BD Pharmingen, Franklin Lakes, NJ; 560845) and FITC-p75^{NTR} (Miltenyi Biotec, Bergisch Gladbach, Germany; 130-091-917) for 30–45 minutes on ice. To stain for PE-RET (Neuromics, Edina, MN; FC15018), the cells were fixed in 4% paraformaldehyde for 10 minutes at room temperature and permeabilized using 0.1% (weight/volume) saponin solution; then they were washed and blocked in PBS with 2% FBS. The cells were then stained with antibodies for 30–45 minutes on ice. Approximately 10 6 cells were stained, and labeled cells were detected using a FACSAria III (Becton

Dickinson Immunocytometry Systems, San Jose, CA). Isotype-matched antibodies were used as controls. FlowJo version, 8.2 (Tree Star), was used to analyze flow data.

For cell sorting, HNK-1/p75^{NTR}-stained cells were washed and resuspended in PBS with 2% FBS. The HNK-1 and p75^{NTR} double-positive cells were enriched by using FACS (BD FACSAria III Cell Sorter). The HNK-1 and p75^{NTR} double-positive cells were gated and sorted using the 4-way purity mode, and the purity of sorted cells was >96%, evaluated by flow cytometry. The sorted NC cells were collected for immunostaining or subsequent experiments. A list of primary antibodies and the working dilutions are provided in [Supplementary Table 2](#).

Immunofluorescence Analysis

For immunocytochemistry, the cells were fixed with 4% paraformaldehyde in PBS at room temperature for 30 minutes, followed by blocking with 1% bovine serum albumin (Thermo Fisher Scientific, Waltham, MA; 23209) with or without 0.1% Triton X-100 (Sigma-Aldrich, T8787) in PBS buffer. Cells were then incubated in primary antibody overnight at 4°C and host-appropriate Alexa Fluor 488 or 594 secondary antibody (Molecular Probes, Invitrogen, Waltham, MA) ([Supplementary Table 2](#)) for 1 hour at room temperature. Cells were then counterstained with mounting medium with 4',6-diamidino-2-phenylindole (Thermo Fisher Scientific, P36931) to detect nuclei. Cells were photographed using a Carl Zeiss confocal microscope (LSM 800). Quantitative image analysis of differentiated neuronal cultures was performed with ImageJ software. A minimum of 4000 cells were analyzed per sample. Percentages of neuronal cells were measured over the total number of cells (4',6-diamidino-2-phenylindole), and the values reported in bar charts represent the mean \pm standard error of the mean.

For section immunohistochemistry, mouse embryos, the innervated HCOs, and HCO explants were fixed in 4% paraformaldehyde in PBS at 4°C, dehydrated, and cryoprotected in 30% sucrose in PBS at 4°C or dehydrated with ethanol series and embedded in optimum cutting temperature compound (Tissue-Tek) or paraffin, respectively. The sections were rehydrated by using standard protocols and microwaved for 15 minutes in target antigen retrieval buffer (Abcam). The sections were then blocked in PBS containing 5% normal donkey serum (Sigma-Aldrich) with 0.5% Triton-X for 1 hour at room temperature, then incubated overnight at 4°C in a mixture of the antibodies against various colon and neuronal markers ([Supplementary Table 2](#)). After washing, the immunosignals were then detected by using the secondary antibody conjugated with Alexa Fluor 488, 594, and 647 (Invitrogen). Sections were photographed using a Carl Zeiss LSM780 or LSM810 confocal microscope.

Plate-Based Single-Cell RNA Sequencing

Plate-based scRNA-seq was performed at the Centre of Genomic Science, University of Hong Kong. For scRNA-seq of human cells, the Smart-seq v4 (Clontech) kit was used

for first-strand synthesis. Single cells were directly sorted into 4 μ l of lysis buffer in a 384-well plate using a FACSAria III flow cytometer (BD Biosciences). First-strand DNA was synthesized within 16 cycles of amplification according to the manufacturer's instructions. Complementary DNA (cDNA) was purified on Agencourt AMPureXP magnetic beads, washed twice with fresh 80% ethanol and eluted in 17 μ l of elution buffer. Then, 1 μ l of cDNA was checked and quantified on an Agilent (Santa Clara, CA) Bioanalyzer high-sensitivity DNA chip. Sequencing libraries were produced by using Illumina (San Diego, CA) Nextera XT tagmentation according to the manufacturer's instructions except with 150 pg of input cDNA, 5 minutes of tagmentation, and 12 cycles of amplification with the Illumina XT 24 index primer kit. Libraries were cleaned by using an equal volume (50 mL) of Agencourt AMPureXP (Beckman Coulter, Brea, CA) magnetic beads and resuspended in 20 μ l of elution buffer. Libraries were checked and quantified on an Agilent Bioanalyzer high-sensitivity DNA chip (size range, 150–2000 base pairs) and by Qubit dsDNA BR (Molecular Probes). Libraries were pooled to a normalized concentration of 1.5 nmol/L and sequenced on an Illumina NextSeq 500 by using the 150-base pair paired-end kit as per the manufacturer's instructions.

Droplet-Based Single-Cell RNA Sequencing

Droplet-based scRNA-seq was performed at the Centre of Genomic Science, University of Hong Kong. For scRNA-seq of mouse cells, the GemCode Single Cell Platform based on the GemCode Gel Bead was used to process the single cells. Chip and library kits (10 \times Genomics) were used according to the manufacturer's protocol. In brief, after cell sorting, cells were partitioned into gel beads in emulsion in the GemCode instrument, followed by cell lysis and barcoded reverse transcription of RNA. Finally, amplification, shearing, and 5' adaptor and sample index attachment were performed. Libraries were purified and sequenced on an Illumina NextSeq 500 as described earlier.

Computational Analysis

Preprocessing of Smart-Seq Single-Cell RNA Sequencing Data. Fastq files with paired-end reads were aligned to the ENSEMBL GRCh38 (release 90, <https://www.ensembl.org/>) human transcriptome by using Bowtie2, version 2.3.4.1¹² with options “-sensitive -mp 1,1 -np 1 -score-min L,0,-0.1 -I 1 -X 2000 -no-mixed -no-discordant -N 1 -L 25 -k 200,” which allows 1 mismatch during sequence alignment. Quality control of the reads of each cell was assessed by using FastQC, version 0.11.6 ([Supplementary Figure 1](#)). Gene expression level was quantified by using TPM values generated by RSEM, version 1.3.0.¹³ For the quality control of the genes and cells, genes that were undetected in all cells and cells that expressed with either fewer than 3000 genes or more than 9000 genes were excluded from the expression matrix for downstream analysis ([Supplementary Figure 1](#)). The distributions of read count and detected gene number in the cells and the fitted sequencing saturation curve are shown in [Supplementary Figure 1](#). Highly variable genes were

selected by fitting a generalized linear noise model (implemented by scikit-learn v0.19.1 Python module; Fabian Pedregosa, CEA Saclay 91191 Gif sur Yvette, France) to the largest difference between the observed and predicted coefficients of variation.¹⁴

Preprocessing of Droplet-Based Single-Cell RNA Sequencing Data. Cellranger toolkit (version 3.0) provided by 10 \times Genomics was used to perform the read demultiplexing and alignment. The unique molecular identifiers were counted by aligning to the mouse mm10 transcriptome. For quality control, only cells with more than 800 detected genes were retained. Genes expressed in more than 10 cells were kept for further analysis. Clustering and marker identification were performed by the Seurat R package.¹⁵

Outlier Detection and Cell Clustering. Because cell outliers can severely affect the clustering, DEG, and gene coexpression analyses, we first removed the cells that were far away from any other cells in the cell population with the method described here. First, dimension reduction was performed by PCA analysis to reduce the effect of the noise genes; then, the Mahalanobis distance between each cell was calculated based on the top 99% variance-explained principal components. The distance between a cell and its k th nearest neighbors was calculated with the following formula:

$$(\text{Distance}_{\text{kth nearest neighbors}})_i = \frac{\sum_{j=k}^{j=k+n} (\text{Distance}_{\text{mahalanobis}})_{ij}}{n}$$

where i is the i th cell, n is the sample size to collect, and j is the j th nearest neighbor. Cells that have the top 5% largest $\text{Distance}_{\text{kth nearest neighbors}}$ values will be considered as outliers. This method can robustly remove the simulated outliers and keep the rare subgroups, and it performs better than existing tools (eg, mvoutlier; Peter Filzmoser and Moritz Gschwandtner, Vienna, Austria), as shown in Supplementary Figure 6.

After removing the outliers, SC3, version 1.7.7¹⁶ was used to cluster the cells using the top 6000 highly variable genes. Markers of each cluster (Supplementary Figure 2) were identified by the get_marker_gene(s) function implemented in SC3. The expressions of the markers were visualized in the form of violin plot by ggplot2 (Hadley Wickham, Houston, TX).

Principal Component Analysis, t-Distributed Stochastic Neighbor Embedding, and SPRING Visualization. Three different methods were used to visualize our scRNA-seq data. All 17,255 protein-coding genes detected in our cells were used to perform the visualization. Feature selection was not performed in this step; thus, less bias was introduced in the visualization. The same pattern was found in all 3 visualization results. PCA and t-SNE were performed by using the prcomp and Rtsne R package (version 3.5.0). SPRING visualization was performed as described previously.¹⁷

Single-Cell Pseudotime Analysis. The SPRING¹⁷ algorithm can robustly capture complex population topologies in scRNA-seq data by force-directed k -nearest-neighbors graphs. After all cells were ordered by the SPRING method, a smooth curve was fitted across the developmental path by principal.curve (R package) (Trevor Hastie, Stanford

University, Stanford, CA). Before curve fitting, outliers were removed by the method described previously. Then, all cells were projected to the smooth curve. The pseudotime of a cell is the distance of its projection point to the beginning of the curve. Finally, the pseudotimes of all cells were normalized to [0, 1].

Species Comparison. After clustering and pseudotime analysis, Spearman correlation was calculated between human clusters and mouse clusters based on the homologous genes. For the pseudotime comparison, we divided the pseudotime into 10 bins and calculated the Spearman correlation between the bins.

Differentially Expressed Genes and Gene Coexpression Network Analysis. DEG analysis was performed by SCDE.¹⁸ Gene Ontology and Kyoto Encyclopedia of Genes and Genomes annotations were performed by clusterProfiler R package.¹⁹ The gene coexpression network (Figure 4H) was constructed by WGCNA²⁰ according to the correlation of the genes. Genes were selected as the overlapping of the TFs in the new markers of the 8 clusters. The gene coexpression network was visualized by Cytoscape software (Paul Shannon, Institute for Systems Biology, Seattle, WA).

All annotated code showing key steps of the analysis are available on GitHub at <https://github.com/ellylab/HCO-paper>.

Derivation of Human Colonic Organoids From Human Pluripotent Stem Cells

Cells were fed mTeSR1 media (STEMCELL Technologies, Vancouver, BC, Canada) and routinely passaged using Dispase II (Gibco, Waltham, MA). ENCCs were generated as described earlier, and HCOs were generated according to a published protocol.²¹ ENCC and HCOs were then combined at an early stage of colon differentiation to generate HCOs containing nerve cells (Figure 6A). Briefly, for induction of definitive endoderm (DE), hPSCs were passaged with Accutase (Invitrogen) and plated at a density of 100,000 cells per well in a Matrigel-coated, Nunclon-surface 24-well plate. For Accutase-split cells, 10 μ mol/L Y-27632 compound (Sigma-Aldrich) was added to the media for the first day. After the first day, the medium was changed to mTeSR1, and cells were grown for an additional 24 hours. Cells were treated with 100 ng/mL activin A for 3 days, and DE was then cultured in hindgut induction medium (RPMI 1640, 2 mmol/L L-glutamine, 2% decomplemented FBS and penicillin-streptomycin) for 4 days with 500 ng/mL FGF4 (R&D Systems, Minneapolis, MN) and 2 μ mol/L CHIR99021 (Tocris) to induce formation of mid-hindgut spheroids. Spheroids were collected from 24-well plates, pooled, mixed with 5000 FACS-sorted ENCCs, and plated in Matrigel at a minimum of 30 spheroids per well. To generate HCOs, spheroids were overlaid with 100 ng/mL EGF plus 100 ng/mL BMP2 (R&D Systems) for 3 days. The medium was then changed twice weekly thereafter. HCOs were replated in fresh Matrigel every 5–7 days at a density of 5–10 organoids per well. Cultures were fed a basic gut medium (advanced DMEM/F12, 1 \times B27 supplement, 1 \times N2 supplement, 10 μ mol/L HEPES, 2 mmol/L L-glutamine, 1 \times penicillin-streptomycin) supplemented with 100 ng/mL epidermal growth factor and maintained in vitro for up to 8 weeks.

In Vivo Transplantation and Ex Vivo Neuromuscular Coupling Test of Human Colonic Organoids

HCOs plus ENCCs were ectopically transplanted into the kidney capsule of NOD/SCID mice by following a previously developed protocol.²² Briefly, 5- to 8-week-old HCOs were embedded in collagen and transplanted into the kidney subcapsular space. Engrafted HCOs were harvested 8–10 weeks after transplantation and subjected to immunohistochemistry for the detection of neural, glial, and colon cells or used for the ex vivo neuromuscular coupling tests.

For the ex vivo neuromuscular coupling test, engrafted HCOs, HCOs plus ENCCs, and HCOs plus SAG-ENCCs were harvested and placed in ice-cold Hank's balanced salt solution. Muscle strips (4–6 mm in length and 1–2 mm in width) were cut from the engrafted HCOs, HCOs plus ENCCs, and HCOs plus SAG-ENCCs. Preparations were suspended isometric-force organ-bath chambers filled with Krebs solution (117 mmol/L NaCl, 4.7 mmol/L KCl, 1.2 mmol/L MgCl₂, 1.2 mmol/L NaH₂PO₄, 25 mmol/L NaHCO₃, 2.5 mmol/L CaCl₂, and 11 mmol/L glucose), warmed at 37°C and with 95% O₂ plus 5% CO₂. After an equilibration period of 60 minutes, the contractile response of the muscle was continuously recorded by using a 4-chamber tissue-

organ bath with isometric-force transducers (AD Instruments Colorado Springs, CO) coupled to a computer equipped with LabChart Pro software (AD Instruments). Muscle preparations were stimulated with dimethylphenylpiperazinium (10 μmol/L, Sigma-Aldrich). Chemical stimulations were applied at 15-min intervals and followed by 3 washes. Tetrodotoxin (10 μmol/L) was applied 5 minutes before dimethylphenylpiperazinium stimulation. The effects of chemical stimulation on tension were evaluated by measuring the area under the curve (AUC). Data are expressed in ΔAUC, that is, stimulated AUC (measured 120 seconds after stimulation) minus control AUC (measured 120 seconds before stimulation).

Statistical Analysis

Statistical significance was determined by the 2-sided unpaired Student *t* test or 1-way analysis of variance using GraphPad Prism 7 (GraphPad Software, San Diego, CA). Tukey posttest was applied for groupwise comparisons. The *P* value is indicated by asterisks in the figures (**P* < .05, ***P* < .01, ****P* < .001). Differences among groups of *P* < .05 were considered statistically significant. All experiments were replicated at least 3 times or from at least 6 embryos. Data are shown as means with standard error of mean.

References

1. **Balaskas N, Ribeiro A, Panovska J, et al.** Gene regulatory logic for reading the Sonic Hedgehog signaling gradient in the vertebrate neural tube. *Cell* 2012; 148:273–284.
2. Böse J, Grotewold L, Rüther U. Pallister-Hall syndrome phenotype in mice mutant for *Gli3*. *Hum Mol Genet* 2002;11:1129–1135.
3. **Chen MH, Wilson CW, Li YJ, et al.** Cilium-independent regulation of Gli protein function by Sufu in Hedgehog signaling is evolutionarily conserved. *Genes Dev* 2009; 23:1910–1928.
4. Ngan ES, Garcia-Barcelo MM, Yip BH, et al. Hedgehog/Notch-induced premature gliogenesis represents a new disease mechanism for Hirschsprung disease in mice and humans. *J Clin Invest* 2011;121:3467–3478.
5. Ellis T, Smyth I, Riley E, et al. Patched 1 conditional null allele in mice. *Genesis* 2003;36:158–161.
6. Xue Y, Cai X, Wang L, et al. Generating a non-integrating human induced pluripotent stem cell bank from urine-derived cells. *PLoS One* 2013;8(8):e70573.
7. **Lai FP, Lau ST, Wong JK, et al.** Correction of Hirschsprung-associated mutations in human induced pluripotent stem cells via clustered regularly interspaced short palindromic repeats/Cas9, restores neural crest cell function. *Gastroenterology* 2017; 153:139–153.
8. Fattah F, Steinbeck JA, Kriks S, et al. Deriving human ENS lineages for cell therapy and drug discovery in Hirschsprung disease. *Nature* 2016;531(7592):105–109.
9. Lee G, Chambers SM, Tomishima MJ, et al. Derivation of neural crest cells from human pluripotent stem cells. *Nat Protoc* 2010;5:688–701.
10. Lee G, Kim H, Elkabetz Y, et al. Isolation and directed differentiation of neural crest stem cells derived from human embryonic stem cells. *Nat Biotechnol* 2007; 25:1468–1475.
11. Zeltner N, Lafaille FG, Fattah F, et al. Feeder-free derivation of neural crest progenitor cells from human pluripotent stem cells. *J Vis Exp* 2014;87:51609.
12. Langmead B, Salzberg SL. Fast gapped-read alignment with Bowtie 2. *Nat Methods* 2012;9:357–359.
13. Li B, Dewey CN. RSEM: accurate transcript quantification from RNA-Seq data with or without a reference genome. *BMC Bioinformatics* 2011;12:323.
14. La Manno G, Gyllborg D, Codeluppi S, et al. Molecular diversity of midbrain development in mouse, human, and stem cells. *Cell* 2016;167:566–580.
15. Butler A, Hoffman P, Smibert P, et al. Integrating single-cell transcriptomic data across different conditions, technologies, and species. *Nat Biotechnol* 2018; 36:411–420.
16. Kiselev VY, Kirschner K, Schaub MT, et al. SC3: consensus clustering of single-cell RNA-seq data. *Nat Methods* 2017;14:483–486.
17. Weinreb C, Wolock S, Klein AM. SPRING: a kinetic interface for visualizing high dimensional single-cell expression data. *Bioinformatics* 2018;34:1246–1248.
18. Kharchenko PV, Silberstein L, Scadden DT. Bayesian approach to single-cell differential expression analysis. *Nat Methods* 2014;11:740–742.
19. Yu G, Wang LG, Han Y, et al. clusterProfiler: an R package for comparing biological themes among gene clusters. *OMICS* 2012;16:284–287.
20. Langfelder P, Horvath S. WGCNA: an R package for weighted correlation network analysis. *BMC Bioinformatics* 2008;9:559.
21. Munera JO, Sundaram N, Rankin SA, et al. Differentiation of human pluripotent stem cells into colonic organoids via transient activation of BMP signaling. *Cell Stem Cell* 2017;21:51–64.
22. Workman MJ, Mahe MM, Trisno S, et al. Engineered human pluripotent-stem-cell-derived intestinal tissues with a functional enteric nervous system. *Nat Med* 2017;23:49–59.

Author names in bold designate shared co-first authorship.